Green Technologies and Sustainability 2 (2024) 100077

Contents lists available at ScienceDirect

Green Technologies and Sustainability

journal homepage:
https://www.keaipublishing.com/en/journals/green-technologies-and-sustainability/

Full-length article

Co-pyrolysis of *Chlorella vulgaris* with plastic wastes: Thermal degradation, kinetics and Progressive Depth Swarm-Evolution (PDSE) neural network-based optimization

Isabel Jia Yen Tan [a,1], Adrian Chun Minh Loy [b,c,1], Bridgid Lai Fui Chin [a,j,*], Kin Wai Cheah [d], Sin Yong Teng [e], Bing Shen How [f], Hatem Alhazmi [g], Wei Dong Leong [h], Huei Yeong Lim [c], Man Kee Lam [c], Su Shiung Lam [i,k]

[a] *Department of Chemical and Energy Engineering, Faculty of Engineering and Science, Curtin University Malaysia, CDT 250, 98009 Miri Sarawak, Malaysia*
[b] *Chemical Engineering Department, Monash University, 3180 Victoria, Australia*
[c] *HICoE-Centre for Biofuel and Biochemical Research, Institute of Self-Sustainable Building, Department of Chemical Engineering, Universiti Teknologi PETRONAS, 32610 Bandar Seri Iskandar, Perak Darul Ridzuan, Malaysia*
[d] *School of Computing, Engineering and Digital Technologies, Teesside University, Middlesbrough TS1 3BX, United Kingdom*
[e] *Radboud University, Institute for Molecules and Materials, P.O. Box 9010, 6500 GL Nijmegen, The Netherlands*
[f] *Biomass Waste-to-Wealth Special Interest Group, Research Centre for Sustainable Technologies, Faculty of Engineering, Computing and Science, Swinburne University of Technology, Jalan Simpang Tiga, 93350 Kuching, Sarawak, Malaysia*
[g] *Carbon Management Technologies Institute (CMTI), King Abdulaziz City for Science and Technology (KACST), P.O. Box 6086, 11442 Riyadh, Saudi Arabia*
[h] *Duriane Professionals Sdn Bhd, 26-1 & 26-3, Jalan Puteri 2/4, Bandar Puteri, 47100 Puchong, Selangor, Malaysia*
[i] *Higher Institution Centre of Excellence (HICoE), Institute of Tropical Aquaculture and Fisheries (AKUATROP), Universiti Malaysia Terengganu, 21030 Kuala Nerus, Terengganu, Malaysia*
[j] *Energy and Environment Research Cluster, Faculty of Engineering and Science, Curtin University Malaysia, CDT 250, 98009 Miri, Sarawak, Malaysia*
[k] *Sustainability Cluster, School of Engineering, University of Petroleum & Energy Studies, Dehradun, Uttarakhand 248007, India*

ARTICLE INFO

Keywords:
Microalgae
Plastic waste
Co-pyrolysis
Kinetic analysis
Distributed activation energy model (DAEM)
Neuro-evolution

ABSTRACT

The search of sustainable route for biofuel production from renewable biomass have garnered wide interest to seek for various routes without compromising the environment. Co-pyrolysis emerges as a promising thermochemical route that can improve the pyrolysis output from simultaneously processing more than two feedstocks in an inert atmosphere. This paper focuses on the kinetic modeling and neuro-evolution optimization in the application of catalytic co-pyrolysis of microalgae and plastic waste using HZSM-5 supported on limestone (HZSM-5/LS), in which co-pyrolysis of binary mixture of microalgae and plastic wastes (i.e. High-Density Polyethylene and Low-Density Polyethylene) was investigated over different heating rates. The results have shown a positive synergistic effect between the microalgae and polyethylene in which the apparent activation energies values have reduced significantly (~20 kJ/mol) compared to that obtained by pyrolysis of individual microalgae component. The kinetic models reflect that the mixture of microalgae and Low-Density Polyethylene for use as co-pyrolysis feedstock requires activation energy that is 23% and 13% lower compared to that required by pure microalgae and the mixture of microalgae and High-Density Polyethylene, respectively. The Progressive Depth Swarm-Evolution (PDSE) was used for neural architecture search, which subsequently provided optimal reaction condition at 873 K can achieve 99.6 % of degradation rate using a tri-combination of LDPE (0.13 %) + HDPE (0.77 %) + MA (0.11 %) in the presence of HZSM-5/LS catalyst.

1. Introduction

With the growing demand for fossil fuels, rapid depletion of fossil fuels such as coal, crude oil and natural gas have garnered considerable concerns [1]. In 2019, more than 80% of the world's total energy consumption was associated with usage of fossil fuels, where the global usage of crude oil was the highest at 31.4%, followed by coal at 26.2% and natural gas at 23.2% [2]. Thus, the increasing consumption of fossil fuels along with the rapidly growing human

* Corresponding author.
E-mail addresses: gembell.iy@gmail.com (I.J.Y. Tan), adrian.loy@monash.edu (A.C.M. Loy), bridgidchin@curtin.edu.my, bridgidchin@gmail.com (B.L.F. Chin), k.cheah@tees.ac.uk (K.W. Cheah), sinyong.teng@ru.nl (S.Y. Teng), bshow@swinburne.edu.my (B.S. How), halhazmi@kacst.edu.sa (H. Alhazmi), leongweidong@gmail.com (W.D. Leong), limhueiyeong@gmail.com (H.Y. Lim), lam.mankee@utp.edu.my (M.K. Lam), lam@umt.edu.my (S.S. Lam).
[1] Authors contributed equally to this work.

https://doi.org/10.1016/j.grets.2024.100077
Received 26 December 2023; Received in revised form 1 February 2024; Accepted 6 February 2024
Available online 7 February 2024

Nomenclature

Abbreviation

ANN	Artificial Neural Network
ARD	Average Relative Deviation
CH_4	Methane
CO_2	Carbon Dioxide
DAEM	Simplified Distributed Activation Energy Models
DTG	Derivative Thermogravimetric
ELU	Exponential Linear Unit
G-20	Group of Twenty
G-DAEM	Gaussian Distributed Activation Energy Models
GHGs	Greenhouse Gases
HDPE	High-Density Polyethylene
HZSM-5/LS	HZSM-5 supported on Limestone catalyst
ICTAC	International Confederation for Thermal Analysis and Calorimetry
IEA	International Energy Agency
LDPE	Low-Density Polyethylene
MA	Pure Microalgae
MAE	Mean Absolute Error
MBE	Mean Bias Error
MSE	Mean Squared Error
MSW	Municipal Solid Waste
NATAS	North American Thermal Analysis Society
PE	Polyethylene
PP	Polypropylene
PS	Polystyrene
PVC	Polyvinyl chloride
RELU	Rectified Linear Unit
RMSE	Root Means Square Error
SELU	Scaled Exponential Linear Unit
TANH	Hyperbolic Tangent Activation Function
TG	Thermogravimetric
TGA	Thermogravimetric Analysis
TGA-FTIR	Thermogravimetric Analysis Coupled with Fourier Transform Infrared Spectroscopy

Notation

A	Pre-Exponential Factor or Frequency Factor
α	The Raw Materials Compositions Converted tnto Products with Respect to Time
β	Heating Rate
C	Reaction Conversion
E_s	Activation Energy
r	Rate of Reaction
T_m	Temperature
$Tmax$	Upper Limit of Reactor Temperature
$Tmin$	Lower Limit of Reactor Temperature
Tr	Reactor Temperature

population and the inevitable human innate's aspirations for higher standard of living have raised substantial concerns on the depletion of non-renewable fossil fuels. In addition, the burning of fossil fuels is acknowledged across the globe as the main contributor to global warming due to the high content of carbon dioxide (CO_2) produced during the combustion process. According to Canadell et al. [3], the amount of CO_2 emission from fossil fuels was predicted to raise *ca.* 1.8%, leading to a new high record of 37.1 billion tonnes of CO_2 emission in 2019. To alleviate such challenges associated with the consumption of fossil fuel, Group of Twenty (G-20) has been initiated to phase out the insatiable consumption of fossil fuel and search for new alternatives renewable energy based on the 12 Principle of Green Chemistry, emphasizing on development of eco-friendly and energy-efficient production of bio-based fuel products [4]. In year 2016, the International Energy Agency (IEA) claimed that more than 30 countries have participated in the renewable energy campaign and the advocated renewable energy sources are solar, biomass and wind power. Notably, the usage of renewable energies has exceeded coal energy and became the largest source of installed power capacity in the world [5].

Biomass is one of the largest contributors to renewable energies, accounting for 12.4% of the energy usage in 2017 [6]. Industrial experts have also forecast that biomass energy will remain as energy resource with the largest growth rate among the other renewable energy in near future, specifically in the period of 2018–2023 [7,8]. Destek and Okumuş [9] have reported that an increase of bioenergy usage from the G-20 countries will stimulate regional economic development and employment by providing new, decentralized and diversified income streams from bioenergy and biomass production. Sulaiman et al. [10] have also reported that an increase of biomass energy in the energy mix of European Union (EU) can mitigate the CO_2 emissions and reduce the global warming potential, resulting in higher energy security and circular economic system. Despite the advantages of biomass energy over conventional fossil fuels, the yield of bio-oil and gaseous products obtained from waste biomass are still low, mainly attributed to the intrinsically high moisture content, high alkali metal and low energy density of wood biomass [11,12].

In recent years, co-pyrolysis technologies have been extensively investigated by researchers as a potential thermochemical method to convert solid biomass into bioenergy. The technology shows several advantages: (1) no expensive chemical reagent (e.g. inert gases) is required for the whole process (2) tunable characteristic (e.g., calorific value, energy density, and stability) of products, and (3) enhancing product quality without the need of further purification steps [12–14]. Fig. 1 shows a comprehensive schematic flowchart indicating the importance of pyrolysis kinetics parameters of a biomass feedstock to the process design, feasibility assessment and scaling up for industrial applications [15]. Generally, the design of pyrolysis processes for biomass requires hydrodynamics and transport simulations including the mass and heat transfer as well as the kinetic parameters information, where the non-isothermal condition kinetic parameters can be easily attained using Thermogravimetric analyzer (TGA) [16–18]. Based on the Scopus® database, the numbers of research work related to the keywords "biomass", "thermogravimetric analysis" and "thermal degradation" have been increasing significantly over the years. The past decade alone (2011–2021 February) have accounted for 2,946 relevant journal articles (Fig. 2). In general, this research field has constantly received increasing interests from the academicians. The average annual increment of the scholarly output is accounted for about 18.25%.

Fig. S 2(a) presents the network map using the full counting method of VOSViewer (https://www.vosviewer.com/) from the keywords extracted from the identified publications. From the network map, it can be clearly seen that there is a significant research cluster (yellow-colored) on kinetic study (Fig. S 1(b)). This indicates that TGA is an analytical tool widely used to investigate the kinetic mechanism of lignocellulosic biomass pyrolysis by the academic community. For instance, Sher et al. [19] have investigated thermal degradation of different biomass feedstock (e.g., rice straw, miscanthus, waste wood, wheat straw and wood pellet) under different reacting agents *via* TGA. They discovered that higher activation energy (E_s) with lower degradation reactivity were attained for biomass (wheat straw and wood pellet) with low cellulosic composition as compared to biomass with high cellulosic composition due to the complexity of cellulose structure (long-chain hydrocarbon). In addition, they reported that the thermal

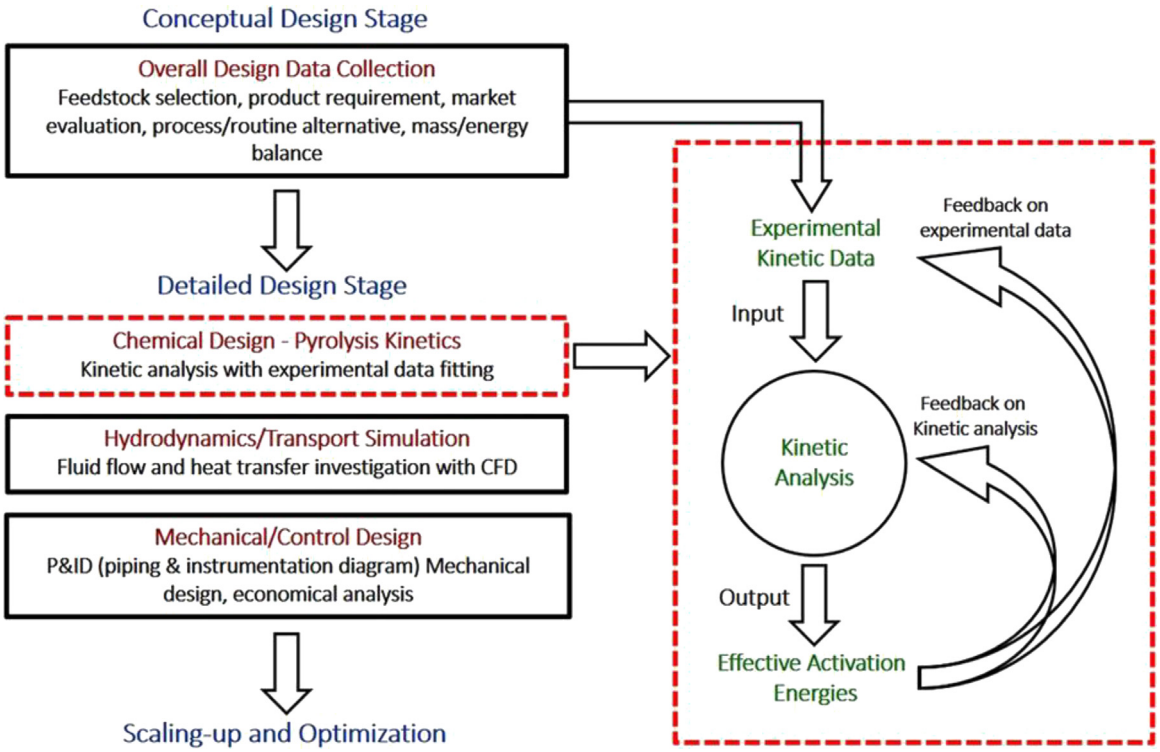

Fig. 1. Schematic flow chart of design of biomass pyrolysis processes [15].

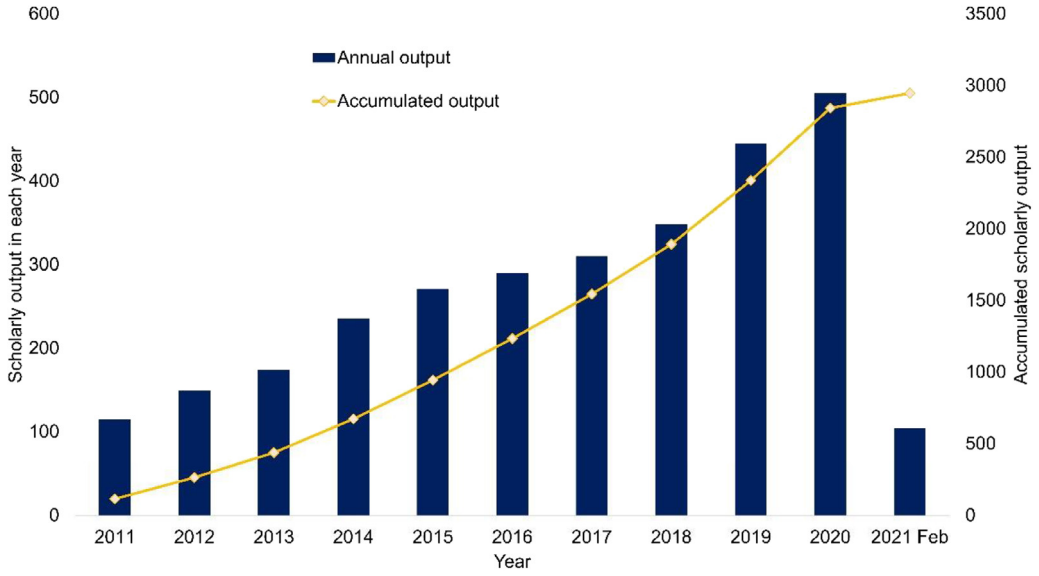

Fig. 2. Trend of journal articles per year which contain "Biomass", "Thermal Degradation" and "Thermogravimetric Analysis" in abstract keywords, and title. *Source:* Adapted from Scopus® database.

decomposition rate regardless of the type of biomass in an inert atmosphere was much slower than that in atmosphere with oxidizing agents. Barzegar et al. [20] have studied the kinetic study of wood biomass in different torrefaction conditions under air and oxy-fuel combustion environments. The study revealed that oxy-fuel combustion can highly affect the decomposition rate of cellulose and lignin components whereas the influence on the degradation of hemicellulose components are negligible, which is in good agreement with previous study [21].

Artificial Neural Network (ANN) is a computational model constructed based on the structure and functions of the biological nerve system, and it has been widely adopted in various application. Its earliest documented application can be back-dated to the mid-1990s, where Kamińnski et al. [37] proposed the use of ANN to model the thermal degradation of vitamin C. The capability of ANN in modeling thermal behavior without the need of pre-determination of the functional relationship between operating parameters and the corresponding outcome has been clearly shown in this work. Progressing to the 21st Century, some researchers have extended the ANN applications in biomass decomposition as shown in Table 1. For instance, Abbas et al. [38] have proposed using neural networks to model the thermal behavior of pulverized coal and biomass by considering three parameters (i.e., fuel atomic ratios, heating rate, and temperature). Their work pointed that the computational economy offered by the neural

Table 1
Summary of application of neural network approach in valorization of waste to bioenergy.

Application	Feedstock	Input parameters	Activation function	Performance function/Error Metrics	Reference
Co-pyrolysis of microalgae and biomass	Mixture of peanut shell and *Chlorella vulgaris*	Heating rate and temperature	Log-sigmoid and the tan-sigmoid	MSE	[22]
Cultural growth of microalgae	Algal biomass	Heating rate, temperature, pH and NO_3 composition	Log-sigmoid	MSE and RMSE	[23]
Extraction of sugars in microalgae via hydrolysis	Mixed microalgal biomass	pH, algal biomass concentration, temperature, and hydrolysis time	Log-sigmoid and the tan-sigmoid	MSE and ARD	[24]
Transesterification of microalgae oil to biodiesel under supercritical methanol condition	*Chlorella CG12*	Reaction time, temperature, and blend ratio	Log-sigmoid	RMSE	[25]
Catalytic degradation of microalgae via pyrolysis	*Chlorella vulgaris*	Heating rate, temperature, and heating duty	Neural architecture is optimized and considers activation functions of softmax, elu, selu, softplus, softsign, relu, tanh, sigmoid, hard sigmoid, exponential and linear.	MSE, RMSE and MBE	[26]
Catalytic pyrolysis of plastic waste	HDPE	Heating rate, temperature, and blend ratio	Tansig–tansig and losig–tansig	MSE, RMSE and MBE	[27]
Synthetic fuel production from pyrolysis of plastic waste	HDPE, LDPE, PP, and PS	Heating rate and plastic composition	Tan-sigmoid	MSE	[13]
Catalytic pyrolysis of plastic waste	LDPE	Heating rate and temperature	Log-sigmoid and tan-sigmoid	MSE, RMSE, and MBE	[28]
Pyrolysis of biomass	Lignocellulosic, forest residue and olive oil residue.	Heating rate and temperature	Log-sigmoid and tan-sigmoid	MSE	[29]
Co-pyrolysis of biomass and coal	Coal gangue and peanut shell	Heating rate, temperature, and blend ratio	Tan-sigmoid	MSE, RMSE, and MBE	[30]
Co-combustion of municipal waste and coal	Paint sludge and australian lignite	Temperature and blend ratio	Tan-sigmoid	MSE and RMSE	[31]
Co-pyrolysis of biomass and municipal waste	Rice husk and sewage sludge	Temperature and blend ratio	Tan-sigmoid	MAE and RSME	[32]
Co-pyrolysis of expired food and plastic mixture	PVC sheath for new and aged cables	Heating rate	Tan-sigmoid	MSE and RMSE	[33]
Co-combustion of biomass and coal	Pine sawdust and lignite coal	Heating rate, temperature, blend ratio	Tan-sigmoid	MSE, RMSE, and MBE	[34]
Thermal oxidative decomposition of biomass	Soybean straw	Heating rate and temperature	Tan-sigmoid	MSE and RMSE	[35]
Co-pyrolysis of biomass	Rice husk	Heating rate and temperature	Log-sigmoid and the tan-sigmoid	MSE and RMSE	[36]

network-based model is significantly better than that developed from conventional tools (e.g., single-reaction devolatilization model). It is then subsequently extended by Conesa et al. [39] to model the thermal decompositions of polyethylene, cellulose and lignin using a multi-layer ANN model. The developed model was trained *via* a backpropagation learning algorithm (i.e., gradient descent algorithm). Their results show that ANN can model the highly non-linear nature of thermal decomposition processes accurately. To-date, ANN-based thermal degradation modeling has been applied to various types of biomass, e.g., forest residue [29], walnut shells [40], sewage sludge [41], *Chlorella vulgaris* [42], and *Nephelium lappaceum L* shell [43]. Most of the works focused on degradation of single biomass, while few studies recently have attempted to use ANN approach to model the co-pyrolysis of simultaneously processing a combination of various materials (e.g. rice husk with sewage sludge [32], *Chlorella vulgaris* with peanut shell [22], corn hub with HDPE [44]; coal gauge with peanut shell [45]; sewage sludge with peanut shell [30]). However, limited works have been reported in determining the optimal ANN topology of thermal degradation or pyrolysis until a method to determine the optimal ANN topology using trial-and-error method in co-pyrolysis of rice husk with sewage sludge has been reported in 2019 by Naqvi et al. [32] using a small number of layers with limited activation function. In the similar year, Teng and co-authors [26] have also proposed a novel Progressive Depth Swarm-Evolution (PDSE) neuro-evolutionary method to replace the trial-and-error method in determining the optimum degradation rate of *Chlorella vulgaris*, resulting in a better prediction accuracy in terms of Root Mean Square Error (RMSE) and Mean Bias Error (MBE) (90% reduction in error), and an excellent R^2 value of 0.999.

To the best of the authors' knowledge, there are two gaps in the literature that should be fulfilled, namely the feasibility of co-pyrolysis of microalgae and plastic waste as source of bioenergy and determination of the precise optimal thermal degradation rate with the aid of Artificial Intelligence. Herein, this paper aims to be a study that provides further understanding of the synergistic effect of co-pyrolysis of *Chlorella vulgaris* with plastic wastes, starting with (Step 1) understanding the recent research development in pyrolysis characteristics of microalgae and plastic waste; (Step 2) selection of suitable feedstock for co-pyrolysis; (Step 3) identifying the pros and cons of the state-of-art iso-conversional kinetics models in literature; (Step 4) selection of the most precise and ideal kinetic models for the study; (Step 5) identifying the kinetic and thermodynamic parameters based on the most ideal model; and (Step 6) identifying the optimum thermal conversion rate of

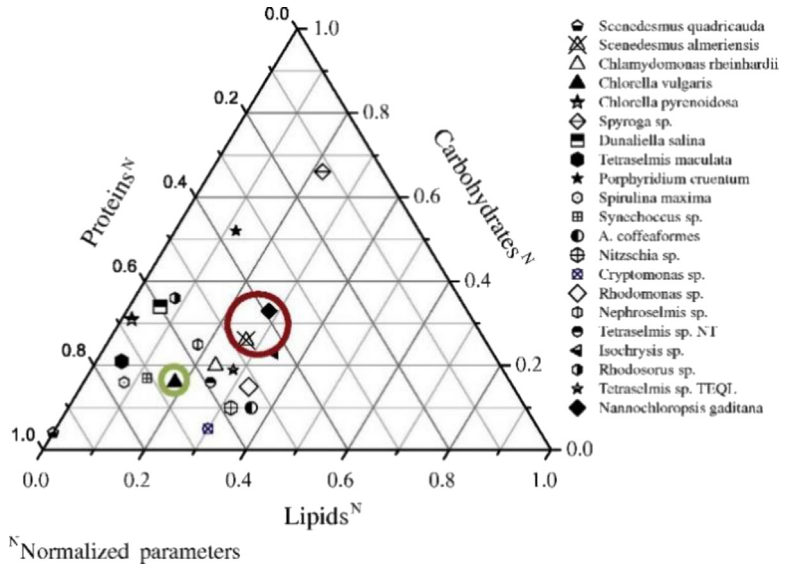

Fig. 3. Ternary diagram with different types of microalgae according to lipid, protein and carbohydrates composition [52].

such co-pyrolysis using neuro-evolutionary approach. The findings can be a key reference to the academic researchers and engineers to identify the bottlenecks and potential improvements in the development of the pyrolysis process by elucidating the synergistic effect of co-pyrolysis and the use of third generation of biofuel feedstock.

1.1. Selection of feedstock

1.1.1. Microalgae (MA)

Up-to-date, the generation of biofuel has evolved to the third generation, where microalgae (MA) are used as raw material for biofuel production. Microalgae is noted as a renewable energy crop with high energy content that requires minimal land area to cultivate [46]. These beneficial properties have successfully made it an attractive source and sustainable alternative for biofuel production [47]. The most abundant microalgae studied for biofuel production are *Cyanophyceae*, *Chlorophyceae*, *Chlorella vulgaris*, *Bacillariophyceae* and *Chrysophyceae* [48,49]. The residues of these microalgae compose carbohydrates, proteins and lipids which can be converted into different types of biofuels such as biodiesel [49], syngas [50] and bio-oil [51] *via* thermochemical conversion. Fig. 3(a) shows a ternary diagram on normalizing the parameters such as lipid, protein and carbohydrate contents of various microalgae [52]. Based on the diagram, microalgae with a high lipid content is more favorable in obtaining a higher bio-oil yield. From Fig. 3, the microalgae strain with the higher lipid content is corresponded to *Scenedesmus almeriensis* and *Nannochloropsis gaditana* (red circle) using *Chlorella vulgaris* (green circle) as a Refs. [52,53]. The rationale behind using *Chlorella vulgaris* as a reference strain in this study is because it is one of the most studied microalgae due to its high productivity and tolerance to environmental factors such as salinity, pH and temperature [54–56].

Since the past decades, researchers started to analyze the thermal degradation rate of microalgae, which aids the pyrolyzer design through the microkinetic data obtained. For instance, the degradation behavior of *Spirulina* under nitrogen and CO_2 atmosphere has been revealed lately by Hong's group [57], claiming that CO_2 atmosphere favored the pyrolysis of algae with high protein content and low lipid content due to the enhanced cracking of the volatile organic compounds during the pyrolysis process. Table 2 shows a series of kinetic models for thermal degradation of microalgae. In 2019, Fong and co-authors have studied catalytic pyrolysis of *Chlorella vulgaris* using various types of catalysts such as HZSM-5 zeolite, limestone, and bifunctional HZSM-5/limestone. Based on the kinetic results, catalytic pyrolysis of *Chlorella vulgaris* over the bifunctional HZSM-5/LS shown a more promising results with a lower average *Es* and ΔH as compared to that pyrolyzed using HZSM-5 and limestone catalysts [58]. Another study from Bui et al. [59], which is a comparative kinetic modeling of thermal degradation of *Chlamydomonas* and *Chlorella sorokiniana*. The five pseudo-components model was found to be the most suitable method to simulate the pyrolysis of microalgae residues as the predicted kinetic data were comparable to previous literature.

1.1.2. Plastic waste

As the world population is growing rapidly, the generation rate of municipal solid waste (MSW) has also increased proportionally. In 2014, approximately 890.8 and 178.6 million tons of wastes were generated in EU-28 member states and China, respectively [76]. The amount of MSW is expected to increase beyond 2.2 billion tons by year 2025, contributing to higher greenhouse gases (GHGs) emission from the disposal of MSW via incineration and landfill [77]. Despite that 70%–80% of the global plastic waste can be recyclable, about 90%–95% of the collected wastes are still disposed *via* landfilling which leads to environmental pollution and land deficiencies [78,79]. From 2004 to 2014, the amount of plastic wastes generated had risen from 225 million tonnes/year to 311 million tonnes/year globally, recording an increment of 86 million tons/year [80]. The recycling of plastic waste is still very low, at which less than 2% of the plastic collected is recycled into the same quality material [81]. Such scenario is ascribed to the complex plastic waste recycling systems with separate collections and several different process design, resulting in a higher waste management cost than the traditional waste processing systems (i.e. incineration and landfill) [82].

Studies have revealed that high pyro-oil yield can be obtained from the pyrolysis of plastics alone with nearly no oxygen content found in the derived oil [83–85]. Therefore, plastics can be considered as a suitable feedstock to produce pyrolysis oils. In 2020, Hu et al. investigated the thermal decomposition of four different plastic (e.g high-density polyethylene (HDPE), low-density polyethylene (LDPE), polypropylene (PP) and polystyrene (PS)) using TGA-FTIR, revealing that CH_4 is the major product from degradation of HDPE, LDPE and PP, while the aromatics and C–H containing compounds are the main products from degradation of PS [86,87]. Mumbach and his team [73] also studied on the thermal degradation behavior of plastic solid waste at four heating rates (278, 283, 293, and 303 K min^{-1}) *via* the deconvolution technique using the asymmetric double sigmoidal function. The simulation profile curves obtained from the simplified kinetic expression based on the

Table 2
Recent TGA pyrolysis for kinetic studies on various microalgae based on mass of sample, final temperature, heating rate, and gas flow.

Types of Microalgae	Mass of sample (mg)	Final temperature (K)	Heating rate (K/min)	Gas flow (mL/min)	Kinetic model	References
Chlorella vulgaris	10	1173	10–100	100	Flynn–Wall–Ozawa (FWO), Kissinger–Akahira–Sunose (KAS), Starink and Vyazovkin	[58]
Chlorella vulgaris	10	1073	5–40	100	FWO and KAS	[60]
Chlorella vulgaris	9	873	10–40	40	FWO and KAS	[61]
Chlorella vulgaris	5	973	10	100	Multiple parallel reaction models	[62]
Chlorella Sorokiniana	5	1000	20	100	five pseudo-components model	[59]
Isochrysis galbana; Nannochloropsis limnetica; and Spirulina platensis	10	1073	10–40	20	Kissinger, Friedman, FWO, KAS, Vyazovkin, Distributed Activation Energy Model (DAEM)	[63]
C. sorokiniana 21; and Monoraphidium 3s35	5	873	20–50	150	DAEM	[64]
Nannochloropsis gaditana and Scenedesmus almeriensis Chlorella vulgaris	8	1273	40	100	Coats Redfern model, Multiple parallel reaction models	[52,65]
and Diplosphaera sp. MM1	5–10	1173	10–30	–	Vyazovkin	[66]
Scenedesmus almeriensis Nannochloropsis gaditana	20	1123–1223	40	200	Volumetric model, Shrinking core model and Random pore model	[67]
Dunaliella tertiolecta	10	1073	5–40	50	FWO	[68]

Table 3
The kinetic and thermodynamic parameters of various types of biomass obtained *via* TGA analysis.

Feedstock	Heating rate (K/min)	*Es* (kJ/mol)	*A* (min^{-1})	ΔH (kJ/mol)	References
Rice husk	10, 20, 30, 50, and 100	175.4	2.939×10^{17}	170.2	[69]
Wolffia arrhiza	10, 30 and 50	170.4	–	165.3	[70]
Sludge Waste	20	181.2	1.77×10^{18}	211.3	[71]
Cherry seed	5,10,20 and 40	274.6	–	–	[72]
Plastic solid waste	5, 10, 20, and 30	170.8	–	163.2	[73]
Coir pith	20	200.1	4.05×10^{15}	200.1	[74]
Wood sawdust	5,10 and 15	181.5	3.83×10^{22}	245.5	[75]
Plum pits	5,10 and 15	136.4	4.20×10^{13}	164.5	[75]
Olive pits	5,10 and 15	108.1	1.42×10^{11}	116.1	[75]
Chlorella vulgaris	10, 20, 30, 50, and 100	156.2	4.83×10^{18}	151.1	[58]

kinetic triplet and deconvolution results were in good agreement with experimental conversion curves, indicating the suitability of PS for pyrolysis. In addition, Table 3 shows that the E_s of plastic waste (170.76 kJ/mol) was much lower than other materials (e.g., cherry seed (274.6 kJ/mol), sewage sludge (181.18 kJ/mol)), showing that plastic waste is much easier to be degraded and more suitable to be a bioenergy feedstock as compared to that of cherry seed and sewage sludge.

1.1.3. Synergistic effect of co-pyrolysis of biomass with plastic mixtures

Co-pyrolysis is a process that involves the degradation of a mixture of two or more materials as feedstocks, in which a positive synergistic effect between molecules will be developed to lower the thermal degradation rate and thus the *Es* of the whole system reduced. Many studies have reported that the co-pyrolysis of biomasses have improved the liquid product yield and purity without any new system configuration or addition of solvent into the system [8,88]. The main advantage of co-pyrolysis method is that it could lower the *Es* of the system, reduce the amount of plastic waste treatment (e.g., incineration and landfills), and maintain the energy security by controlling the volume of plastic waste removed (Table 4). Over the decades, researches have reported the benefits of co-pyrolysis techniques as compared to conventional pyrolysis of biomass [89,90]. For instance, Chen et al. [90] studied the co-pyrolysis behavior of tobacco straw and polypropylene mixture, and they found that the addition of polypropylene enhances the gas production associated with the reduction of E_s compared to pyrolysis of tobacco straw individually. In addition, Wang et al. [91] have reported that co-pyrolysis of plastic and biomass shows a higher heating values than the conventional pyrolysis as the char content in the mixture enhances the catalytic reactivity by decreasing the pyrolysis temperature, with an enhancement by a positive synergistic effect developed by the plastic-biomass mixture. Moreover, the addition of polypropylene (PP) was found to promote the pyrolysis process of biomass by lowering the active zone peak pyrolytic temperature of degradation, where additional reaction radicals can be formed during co-pyrolysis: initiation, formation of secondary radicals (depolymerization, formation of monomers, favorable and unfavorable hydrogen transfer reactions, intermolecular hydrogen transfer (formation of paraffin and dienes), isomerization, *via* vinyl groups), and termination by disproportionation or recombination of radicals [92–94].

Plastic wastes are attractive feedstock for co-pyrolysis due to their low oxygen and higher hydrogen content [94]. Especially, the municipal plastic wastes (e.g., PE, PP and PS) are hydrocarbons without any oxygen linkage. Thus, high hydrogen content with low or zero oxygen content in the plastic wastes could compensate for the intrinsic hydrogen deficiency in biomass to produce pyrolysis-oil with higher heating values [97]. In 2016, Chattopadhyay et al. [98] have studied catalytic co-pyrolysis of biomass and plastics blends in fixed-bed reactors. A positive synergistic effect between biomass and plastics was observed, where the formation of liquid and gaseous products was gradually increased with the rise in the plastic blending ratio. Based on their

Table 4
Comparison of different co-pyrolysis methods to obtain pyrolysis oil [8,14,95,96].

Upgrading methods	Operating conditions	Process description	Advantages	Disadvantages
Hydrocracking or hydrogenolysis	Severe conditions (>300 °C, 1–10 MPa), it requires H_2 donor solvents, catalyst ($NiAl_2O_3$, TIO_2).	It involves both hydrogenation and cracking; reduce the molecules to the smallest carbon chain	It gives room for large quantities of light products	High cost, it needs complicated equipment, catalyst deactivation, reactor clogging
Co-pyrolysis	Moderate temperature (400–600 °C); two or more feedstock materials at optimal mixing ratio, absence of gasifying agent; mild pressure and moderate heating rate; introduction of inert gas such as nitrogen or argon; and short residence time of vapor product.	It involves three basic steps (samples preparation, co-pyrolysis, and condensation), two or more feedstock materials, moderate operating conditions, absence of oxygen (O_2)	Simple, safe, and effective approach for production of a high-grade pyrolysis oils due to the synergistic effects between the constituent feedstocks.	Pre-treatment process of feedstock is needed, which is time and energy consuming.
Emulsification	Mild conditions, surfactant is needed	Can be combined with diesel for bioenergy usage. Bio-oil is highly miscible, mixable with petrochemical fuels with the presence of surfactants	Simple and less corrosive	Requires high energy for production
Gasification	High temperature (700–900 °C). Gasifying agent is essential and high heating rates.	It involves gasifying agent such as steam or O_2. High temperature is needed to break the biomass molecules and then react with the H_2O molecules to form bio-oil or syngas.	High maturity	Low yield of bio-oil production and more energy is required.
Supercritical	Mild conditions, organic solvents are needed such as alcohol, acetone, ethyl acetate, glycerol	Enhance the reaction through its unique transport properties: gas-like diffusivity and liquid-like density.	Higher oil yield, better fuel quality (lower oxygen content and lower viscosity)	High operating and maintenance cost.

findings, the optimum performance (i.e., yielding 47 vol% of hydrogen (H_2) gas) can be obtained by setting the biomass-to-plastics ratio at 5:1 under the presence of 40% Co/30% CeO_2/30% Al_2O_3 catalyst and heating rate of 10 K/min. Moreover, Jin et al. [99] have studied the synergistic effects of biomass and plastic co-pyrolysis and pyrolysis kinetics using a thermogravimetric analyzer. Based on their results, a positive synergistic effect on product yields is observed under non-sooty conditions, resulting in higher char yields with lower tar yields. Whereas co-pyrolysis under sooty conditions inhibits the formation of gases products and soot (solid char) formation, resulting in higher tar yields and different soot morphologies (lesser yield).

2. Materials and methods

In this work, binary mixture of microalgae and plastic waste was selected to demonstrate the feasibility of co-pyrolysis *via* kinetic modeling and neural network approaches. The research methodology and procedures are shown in Fig. 4, which includes a description of the TGA experimental procedures (Section 2.1), selection of the most suitable kinetic model for the binary mixture of microalgae and plastic wastes valorization (Section 2.2), and followed by the empirical data optimization using neuro-evolution method (Section 2.3).

2.1. Thermal degradation experimental procedures

The experimental set up for degradation of MA, MA with HDPE, and MA with LDPE mixtures under non-isothermal condition at 5 different heating rates (e.g 10 K/min, 20 K/min, 30 K/min, 50 K/min, and 100 K/min) is shown in Fig. 5. The pure microalgae ash "*Chlorella vulgaris*" (MA), HDPE, and LDPE were obtained from Centre for Biofuel and Biochemical Research, Universiti Teknologi PETRONAS (UTP) and Shen Foong Plastic Industries Sdn Bhd, Malaysia. The physiochemical properties of the MA, HDPE, LDPE feedstocks such as volatile matter, ash content and fixed carbon were analyzed based on BS EN 14774-3:2009, BS EN 14775:2009, BS EN 15148:2009 standards, as provided in Table S1. The HZSM-5/LS catalyst was prepared based on wetness impregnation method reported in our previous studies [58,69]. Zeolite (HZSM-5) and Limestone (LS) powders were obtained from Merck Sdn Bhd and Calrock Sdn. Bhd, respectively. Firstly, the limestone was annealed at 1173.15 K (900 °C) for 4 h to convert the calcium carbonate ($CaCO_3$) into calcium oxide (CaO). The bifunctional HZSM-5/LS catalyst was prepared using 5 g of aqueous HZSM-5 mixed with 100 mL of deionized water. Subsequently, LS (5 g) was added into the suspension under continuous stirring. The resultant suspension was treated by ultrasound for a duration of 0.5 h. Lastly, the mixture of HZSM-5/LS was dried at temperature of 353.15 K for 12 h and calcined at temperature of 873.15 K for 3 h. During the experiment, an approximate 5 mg of well-mixed sample of Pure MA, HDPE, and LDPE as well as binary mixtures of HDPE/MA or LDPE/MA with a mass ratio of 50/50 were placed in a ceramic crucible and introduced into the system. The mass ratio was based on the optimum ratio given by previous studies [100–102], where 50/50 (MA: Plastic waste) was the ratio to attain maximum yields of alcohols and hydrocarbons *via* thermal degradation. Then, the equipment was pre-heated to 353.15 K under a continuous N_2 flow of 100 mL/min to remove the unwanted or trapped gases in the system before starting the pyrolysis from 353.15–1173.15 K. Each experimental run was repeated for at least thrice to ensure the reliability and repeatability of the obtained data.

2.2. Selection of kinetic models

Table 5 shows a series of model free (iso-conversional) and model fitted methods recommended by International Confederation for Thermal Analysis and Calorimetry (ICTAC) and also the state of art kinetic models that have been discovered in recent years [105–107]. All the kinetic parameters obtained through non-isothermal conditions and the derivations of the models are shown in Table S.1. The main advantages of non-isothermal conditions are easy to control the range of temperature set, eliminate the error caused by thermal induction period, and permit a rapid scan of the whole temperature range of interest [107–109].

Amongst all the models proposed, the distributed activation energy model (DAEM) is the most favorable and precise method because it can calculate the E_s and A of a complex reaction such as microalgae with a boundless number of non-reversible first order homologous

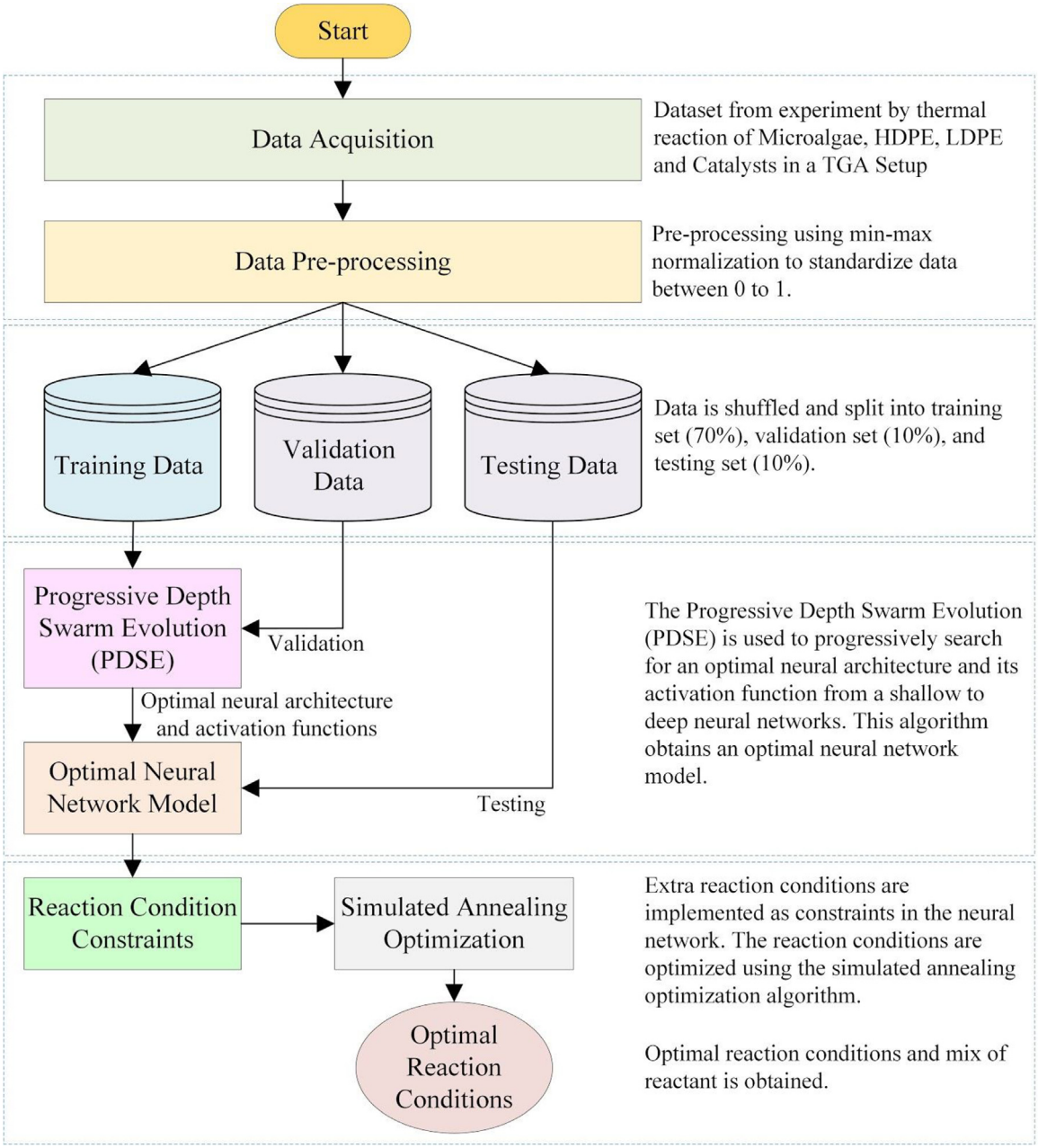

Fig. 4. Schematic flow chart design of the co-pyrolysis of microalgae and plastic waste binary mixture.

reactions [122]. DAEM is widely used in the pyrolysis of lignocellulosic biomass to determine the kinetic parameters of multiple reactions through the assumption of simultaneous first-order reactions [123]. There are various methods in solving the DAEM to initiate the kinetic parameters in the present literature. For example, an asymptotic method was used to construct an exact approximation to each of the integrals to obtain the solutions at a faster rate by reducing the computation time [124,125]. Cai and Ji [126] have also applied a pattern search method to evaluate the kinetic parameters of DAEM. Notably, they have found out that the frequency factor ($A = A_0 T_m$) is a function of temperature and thus, the approximation of temperature integral can be upgraded by fixing the semi-empirically tuned numerical parameters in the range of $4 \leq u' \leq 200$ and $-2.5 \leq m \leq -2.5$ to improve the accuracy of the model (G-DAEM) [125,126].

Thermodynamic parameters [i.e. enthalpy change (ΔH), Gibbs free energy (ΔG) and entropy change (ΔS)] can be computed after obtaining the kinetic values. The enthalpy is known as a system's heat content whereas the change in enthalpy energy (ΔH) defines the amount of energy that enters to or exits from the system during the co-pyrolysis process where $+\Delta H$ indicates an endothermic reaction and $-\Delta H$ indicates an exothermic reaction. Furthermore, the Gibbs free energy (ΔG) is the measure of the maximum reversible work that can be done in a thermodynamic system. According to National Math and Science Initiative [127], $-\Delta G$ means that the process is thermodynamically favorable and will occur spontaneously whereas $+\Delta G$ shows a thermodynamically unfavorable reaction. The change in entropy (ΔS) is to measure the randomness or disorder in a system; a negative value suggests that there is less dispersal meanwhile a positive value means that there is more dispersal. Few studies from literatures had conducted thermodynamic analyses on the co-pyrolysis of biomass and plastic waste mixtures [44,87].

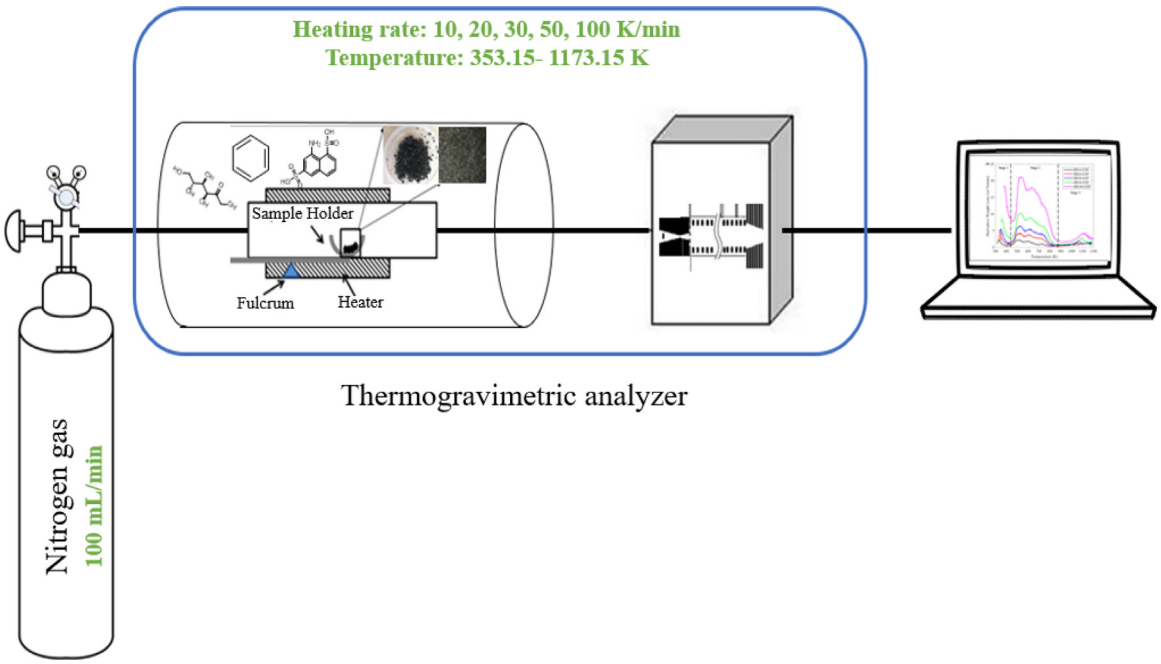

Fig. 5. Experimental setup of the co-pyrolysis process using TGA.

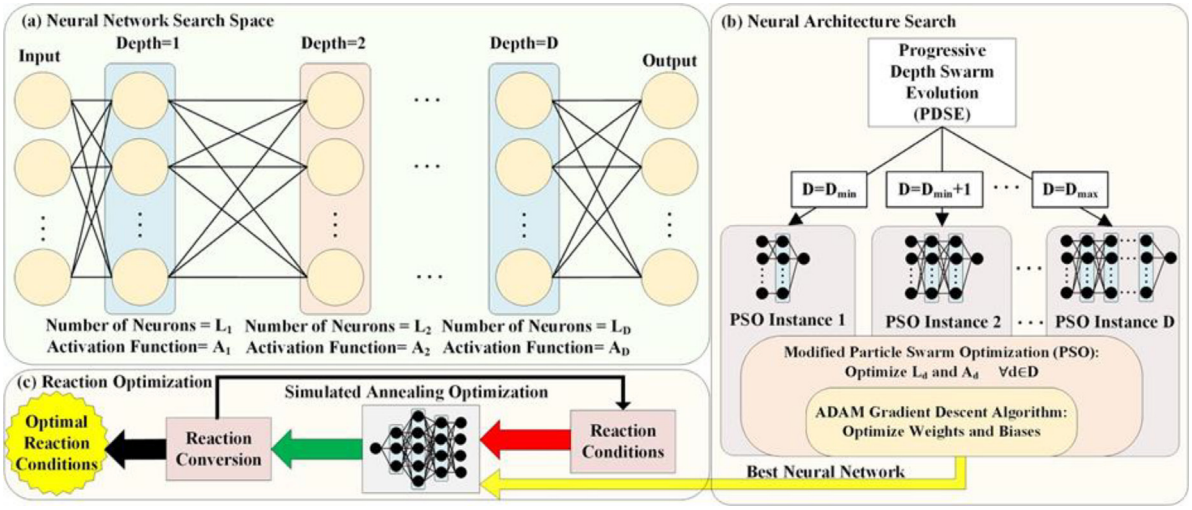

Fig. 6. (a) Variable depth neural network as the neural network search space (b) Neural architecture search using Progressive Depth Swarm Evolution (PDSE) (c) Reaction optimization using simulated annealing algorithm.

2.3. Neural network architecture search and reaction condition optimization

This work presents the neuro-evolution approach for TGA modeling [26]. This approach uses the Progressive Depth Swarm Evolution (PDSE) algorithm which progressively searches from a shallow neural network to a deep neural network with maximum depth of 10. The neural network search space model was constructed using a variable depth neural network as shown in Fig. 6(a). The depth of the search space model can be varied to give a neural network of different depths, number of neurons (unique for each layer), and activation functions (unique for each layer). The activation functions that were optimized in this work (during neural architecture search) include softmax, elu, selu, softplus, softsign, relu, tanh, sigmoid, hard sigmoid, exponential and linear activation functions.

In this work, six input variables of the neural network were chosen to be manipulated as follows: mass fraction of HDPE as reactant, mass fraction of LDPE as reactant, mass fraction of microalgae as reactant, presence of catalyst, heating rate of the reactor and reactor temperature meanwhile the output of the reactor refers to the remaining mass percentage of the reactants. The loss of the ANN was chosen to be measured using Mean Absolute Error (MAE), ensuring that the errors were proportional to the reaction variables. Additionally, Mean Bias Error (MBE), Root Mean Square Error (RMSE) and R^2 value were also used as validation metrics. As ANN are mathematically differentiable models, training of weights and bias benefit greatly from using stochastic gradient descent algorithms [128]. Therefore, the weights and biases

Table 5
Mathematical equations of different model fitting and model free kinetic methods.

Method	Equation	Remarks	Ref
Kissinger	$\ln\left(\frac{\beta}{T_m^2}\right) = \ln\left(\frac{AR}{E_s}\right) - \frac{E_s}{RT_m}$	Kissinger is the first iso-conversional method reported in literature where the *Es* of each conversion value are fully utilized to evaluate kinetic parameters. This is because it assumed that *Es* does not vary according to the conversion rate and thus, its accuracy is low. The accuracy of the Kissinger method is limited to about 1% as it is accurate only for first order reaction.	[103–105]
Ozawa–Flynn–Wall (FWO)	$\ln(\beta) = \ln\left(\frac{AE_s}{g(\alpha)R}\right) - 5.331 - 1.052\frac{E_s}{RT}$	FWO method is used to predict the *Es* as a function of the reaction conversion over the whole temperature domain. However, the accuracy of the FWO method is not satisfactory because of the crude temperature integral approximation.	[106,107]
Kissinger–Akahira–Sunose (KAS)	$\ln\left(\frac{\beta}{T^2}\right) = \ln\left(\frac{AR}{g(\alpha)E_s}\right) - \frac{E_s}{RT}$	A simplified temperature integral approximation is used in the derivation. The method is derived based on the assumption of a constant *Es* from the start of the reaction to the conversion degree. Thus, KAS method offers great improvements in terms of predicting more accurate *Es* values when compared to FWO method.	[108–110]
Friedman	$\ln\left(\frac{d\alpha}{dt}\right) = \ln[Af(\alpha)] - \frac{E_s}{RT}$	Friedman technique is a widely used iso-conversional method due to its simplicity and high accuracy. Although this technique is sensitive to data noise, the noise effect can be minimized by considering not solely on the data for a specific degree of conversion. This method makes no mathematical approximations and considered that conversion functions f (α) remain constant which indicates that sample decomposition is depends solely on loss of mass rate. The systematic error in evaluating the *Es* is reduced as the method is independent from the range of heating rates.	[111–113]
Starink	$\ln\left(\frac{\beta}{T^{1.92}}\right) = \text{Constant} - 1.0008\frac{E_s}{RT}$	Starink method is more accurate than KAS and FWO method. This is because the approximation of the temperature integral is highly precise and accurate. In real case, this approximation has eventually no significant effect on the accuracy of the method when applied to practical data. Amongst KAS, FWO, Friedman and Kissinger that provide *Es* directly from the gradient (i.e. with the absence of the iterative procedures) the Starink method provides the best accuracy of *Es* analysis methods.	[114–116]
Weighted Average Global Method	$\ln\left[\frac{g(\alpha)}{T^2}\right] = \ln\left(\frac{AR}{\beta E}\right) - \frac{Es}{RT}$ $AverageEs = \frac{X_2}{X_2+X_3}E_2 + \frac{X_3}{X_2+X_3}E_3$	Weighted average global model is grouped under model fitting method based on the two-stage reaction kinetic scheme to achieve the global kinetic parameters from biomass combustion. The kinetic scheme is calculated using Coats-Redfern method.	[117,118]
Distributed activation energy model (DAEM)	$\ln\left(\frac{\beta}{T^2}\right) = \ln\left(\frac{AR}{E_a}\right) + 0.6075 - \frac{E_s}{RT}$	DAEM method is one of the multi-reaction models used widely to clarify the thermal decomposition of biomass. DAEM has a better universality in kinetic modeling of material degradation process such as plastic waste, municipal solid waste, rice husk, microalgae; regardless how complicated is the system.	[119–121]

for each neural network in the PDSE algorithm are inertly optimized using the popular ADAM gradient descent algorithm [129]. For neural architecture search, the PDSE algorithm shown in Fig. 6(b) was being searched from an ANN model with low to high depth using the multiple modified particle swarm optimization instances to optimize the number of neurons and activation functions for each specific layer [128–130]. Since the neural architecture search problem was an *NP*-hard problem which suffers from the exploitation–exploration dilemma [131], our PDSE algorithm was designed to have hyper-parameters which balances exploration and exploitation in neural architecture search. Firstly, the maximum number of neural networks evaluated per depth was constrained (at 1000 in this work) to represent a control hyperparameter for search exploitation. The depth range (1 to 10 in this work) also provides a control hyperparameter to limit the exploration space. Both maximum number of neural networks evaluated per depth and depth range can be adjusted according to the computational power of the processing unit. Therefore, the PDSE algorithm can provide an adjustable exploration and exploitation to search for an optimal neural network model.

After the best neural network model was obtained from the PDSE algorithm, the simulated annealing algorithm [132] was used to optimize the reaction conversion by manipulating the reaction conditions by using the best neural network as the surrogate model. The simulated annealing acts as a stochastic solver which solves the optimal reaction

condition treating the neural network as a "Blackbox" model, which is presented in the 5 steps below.

Step 1: Generate initial solution (reaction conditions) randomly.

Step 2: Find a neighbor solution for each of the initial solutions.

Step 3: Stochastically choose a solution between the initial and neighbor solution based on the probability, $p = \exp(-\frac{Fitness_{neighbour} - Fitness_{initial}}{Temperature})$.

Step 4: Linearly decrease the temperature.

Step 5: Repeat from step 2 if the termination condition is not met.

For the optimization formulation, a mass fraction constraint was introduced to ensure that the mix of reactant mass fraction sums up to one. The main objective of this optimization analysis is to maximize the conversion in various reactor temperature range as expressed in the equations below:

$$Max\ C = 1 - Mass\ Remaining\ (in\ Fraction) \tag{1}$$

$$Subjected\ to: \sum_{r}^{R} F_r = 1 \tag{2}$$

$$Tmin \leq Tr \leq Tmax \tag{3}$$

where C is the reaction conversion, F_r is the mass reaction of reactant $r \in R$, Tr is the reactor temperature, $Tmax$ and $Tmin$ is the upper and lower limit for the range temperature range, respectively.

3. Results and discussion

3.1. Thermal degradation behavior of microalgae and polyethylene

3.1.1. Microalgae (MA)

The results for pyrolysis of only MA at different heating rates of 10 K/min, 20 K/min, 30 K/min, 50 K/min and 100 K/min were used to plot the thermogravimetric (TG) and derivative thermogravimetric (DTG) curves as shown in Fig. 7(a) and Fig. 8(a), respectively. Three stages of degradation can be observed from the degradation profile: Stage I (water evaporation and dissipation of light volatile compounds stage) occurs at temperatures ranging from room temperature (~298 K) to approximately 460 K; Stage II (main decomposition stage to yield volatile matter) occurs at temperature of 460–830 K, and Stage III (high temperature decomposition stage) occurs at above 830 K. The temperature range specifically in stage II where the main decomposition takes place was taken according to DTG curves and summarized as shown in Table 6. The initial temperature where stage II begins was denoted as T_0, while the final temperature where stage II ends and stage III begin is denoted as T_f. Lastly, the peak temperature where the maximum temperature achieved in stage II is denoted as T_p.

Fig. 7(a) shows that the trends of TG curves at all different heating rates were almost identical: there is a slight decrease of weight loss in Stage I (15 wt%), then a rapid loss of weight during Stage II (47 wt%), followed by a constant weight loss in Stage III. Similarly, the trend in DTG curve showed in Fig. 8(a) was similar for all heating rates of 10–100 K/min, where there are two significant peaks observed at 500–800 K. Other minor peaks in the temperature range indicate the degradation of protein, carbohydrate and lipids [133]. According to Chen et al. [134], the peak, shoulder and long tailing shown in the DTG curves indicate different degradation mechanisms of MA. The overlapping of the significant peaks leads to the formation of shoulder, which represents the rapid decomposition of hemicellulose structure meanwhile the peak and tailing indicate the cellulose and lignin decomposition, respectively.

Such finding was in a good agreement with those previous studies on pyrolysis of MA (e.g., *Chlorella pyrenoidosa*, *Chlorella vulgaris*, and *Chaeodacrylum tricomutum*), in which two similar major peaks were observed in Stage II of degradation, suggesting that the MA species tend to have more than one major peak in Stage II of degradation [59,63,65,135]. Whereas, comparing with the DTG profile of other types of biomass (e.g. pine sawdust, sawdust, Areca nut husk, fern stem and sugarcane straw), only one major peak can be observed during Stage II or known as the active zone of degradation [134,136–138]. The peak intensity shown in the DTG curve represents the reactivity of the samples during pyrolysis reaction; a low peak intensity indicates that a complete thermal degradation process can be achieved faster due to lesser energy required in the system. Thus, the difference in peak intensity observed in this study was due to the different decomposition mechanisms of organic and inorganic constituents, length and distribution of chains within the constituents and the pyrolytic conditions of the system.

3.1.2. Polyethylene

From Fig. 7(b) and 7(c), the trend of TG curves of pure LDPE and HDPE were slightly different from that of pure MA (70%), in which the weight loss reached almost 100%, regardless the heating rates. This is due to that the pure MA has a higher ash and fixed carbon content, resulting in a higher residue remaining at the end of the pyrolysis (10–40 wt%) as compared to polyethylene (*ca.* 0 wt% for LDPE; < 5 wt% for HDPE). These results were consistent with those studies reported previously by other authors on the TG trends of plastic wastes and biomass [98,139]. As shown in Fig. 8(b) and 8(c), the main degradation of both LDPE and HDPE occurred at the temperature range of 500–830 K. Unlike the pyrolysis of MA, the decomposition of pure LDPE and HDPE exhibited only one narrow degradation stage and degraded at a higher temperature of 500 K. Whereas, the decomposition of MA started to decompose at a lower temperature of 300 K and consisted of three decomposition stages. Such discrepancies in TG profile can be attributed to the strong structural composition of pure MA (i.e. protein, carbohydrate, and lipid) that need a higher temperature to be degraded, which could not be find in LDPE and HDPE molecules.

However, there were slight differences shown in the DTG curve of HDPE as illustrated in Fig. 8(c) when compared to that of LDPE. By observing the DTG trends of HDPE, there were multiple peaks observed at heating rates of 10–20 K/min, while only one major peak can be observed at heating rates of 30–100 K/min. Whereas, the DTG trend of LDPE in Fig. 8(b) only shows one major peak for every heating rate. Such slight differences in DTG curves of HDPE and LDPE were mainly due to the difference in volatile matter content and the tensile strength of both samples. According to Dewangan et al. a higher volatile matter is found in LDPE which provides a higher volatility and reactivity over HDPE [139]. Meanwhile, HDPE has a higher tensile strength as opposed to LDPE and hence, the intermolecular forces within the polymer chain of HDPE are stronger and more complex to be depolymerized [98].

3.1.3. Co-pyrolysis of MA and polyethylene mixtures

From the TG results of co-pyrolysis of MA and polyethylene blends as illustrated in Fig. 7(d) and 8(f), the weight loss obtained in the co-pyrolysis was much higher as compared to that of solely MA. For instance, *ca.* 10 wt% and 15 wt% of the residue were remained at the end of co-pyrolysis of LDPE with MA and HDPE with MA mixture, respectively. A minor weight loss of *ca.* 5 wt% for both LDPE and MA mixture was observed at the temperature region of 300–450 K, followed by a continuous rapid decrement of weight loss of 85–90 wt% occurred from 450 K to 830 K and lastly, an almost constant trend in remaining residue (*ca.* 10 wt% for 20–100 K/min; < 10 wt% for 10 K/min). Comparably, a similar trend can be observed from the TG curve of HDPE/MA blends as well, where the decomposition began from 300 K to 450 K with a maximum weight loss (15–60 wt%), the weight then dropped sharply at 450–830 K with an approximation of 75–80 wt%, and reached constant at temperature above 830 K (> 10 wt% for 30 K/min; ≤ 10 wt% for remaining heating rates). From the results, it can be concluded that LDPE/MA blend decomposed more during stage II as compared to HDPE/MA blend. Since LDPE has a

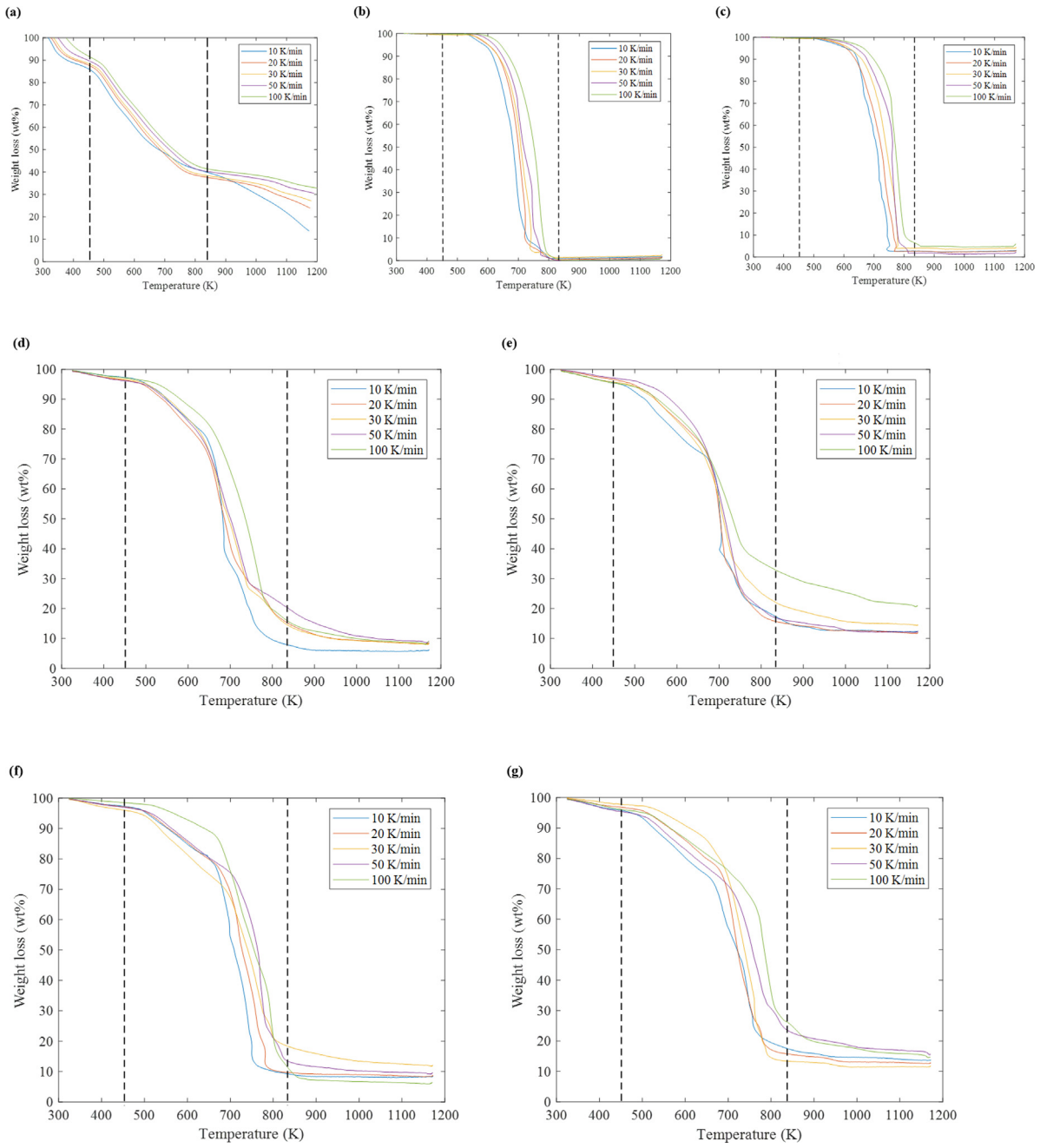

Fig. 7. TG graphs of (a)–(c): non-catalytic pyrolysis of pure MA, pure LDPE and pure HDPE; (d) non-catalytic co-pyrolysis of LDPE/MA, (e) catalytic co-pyrolysis of LDPE/MA with bifunctional HZSM-5/LS catalyst, (f) non-catalytic co-pyrolysis of HDPE/MA, and (g) catalytic co-pyrolysis of HDPE/MA with bifunctional HZSM-5/LS catalyst.

slightly higher volatile matter content and relative volatility than that of HDPE, and thus LDPE/MA blend was more readily decomposed into volatile hydrocarbons than HDPE/MA blend during the second stage of co-pyrolysis process [140].

By observing the trends of DTG curves for LDPE/MA and HDPE/MA co-pyrolysis process as indicated in Fig. 8(d) and 8(f), the rate of weight loss over time (dw/dt) for both mixtures were lower than that of pure LDPE and HDPE. The maximum rate of weight loss over time of LDPE decreased from 140 wt%/min to about 75 wt%/min at 100 K/min, while maximum *dw/dt* of HDPE reduced from 125 wt%/min to *ca.* 90 wt%/min at the same heating rate when compared with the *dw/dt* of co-pyrolysis. This is due to the slow *dw/dt* rate of pure MA where the maximum *dw/dt* rate was only 22 wt%/min at 100 K/min. This clearly indicates the pyrolysis of pure MA has a slower *dw/dt* rate, where the highest *dw/dt* rate achieved was only 22 wt% at 100 K/min. This suggests that the presence of MA in the co-pyrolysis process leads to a positive synergetic effect in reduction the degradation rate of LDPE and HDPE in the blending mixtures, which is supported by previous studies [141,142].

3.2. Catalytic co-pyrolysis of MA and polyethylene mixtures

As demonstrated in Fig. 7(e) and 7(g), the TG trends for catalytic co-pyrolysis of MA and polyethylene blends were very similar to that of co-pyrolysis of the mixtures without the presence of catalyst. Likewise, the decomposition started from 100 wt% to 95 wt% at temperature of 300–450 K, and then underwent a rapid decomposition at the stage II where most of the weight losses occurred, lastly reached an almost constant at the end of the process. As reported, the addition of the catalyst is to enhance the desire product by reducing the apparent

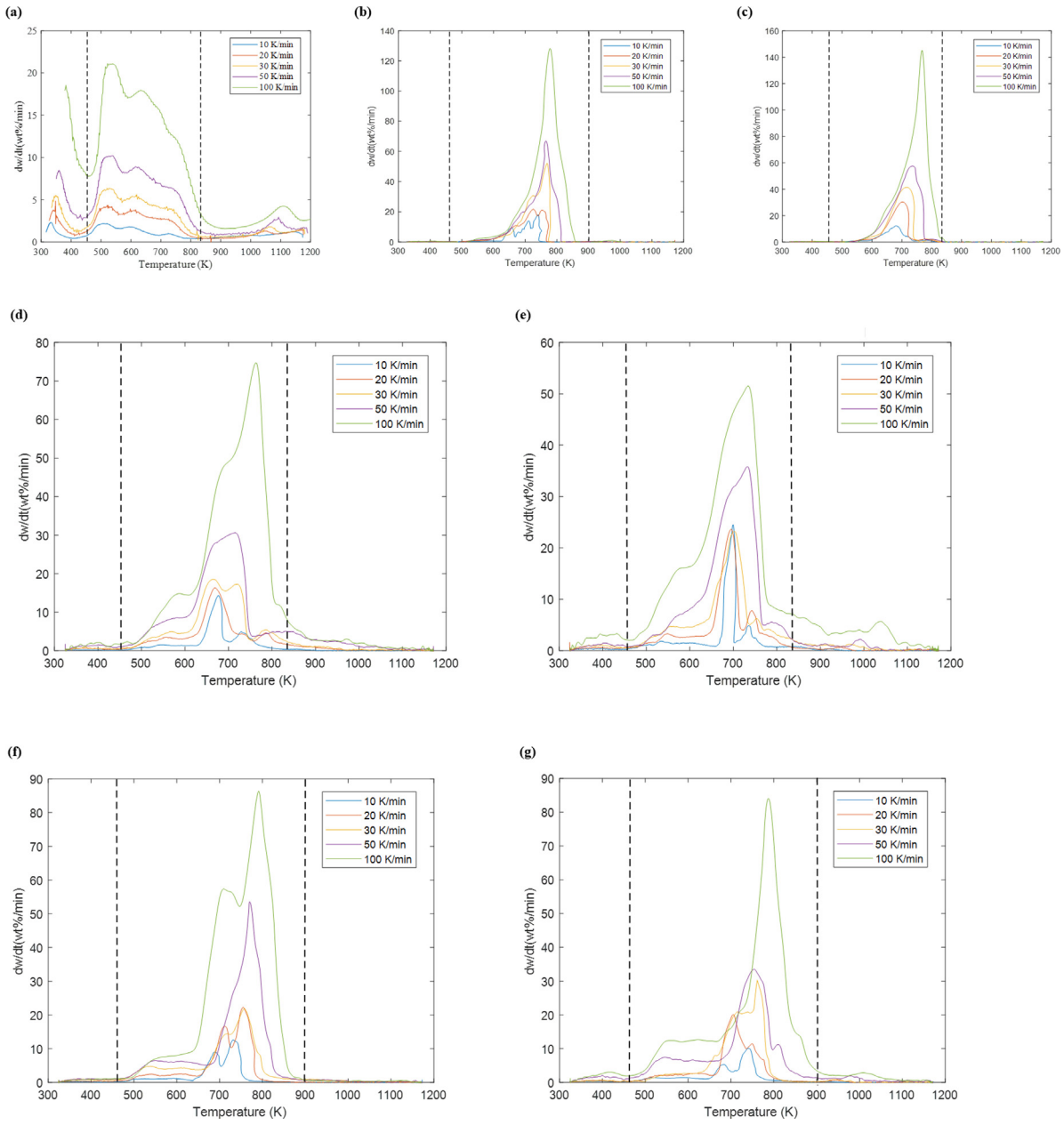

Fig. 8. DTG graphs of (a)–(c): non-catalytic pyrolysis of pure MA, pure LDPE and pure HDPE; (d) non-catalytic co-pyrolysis of LDPE/MA, (e) catalytic co-pyrolysis of LDPE/MA with bifunctional HZSM-5/LS catalyst, (f) non-catalytic co-pyrolysis of HDPE/MA, and (g) catalytic co-pyrolysis of HDPE/MA with bifunctional HZSM-5/LS catalyst.

Es required of the co-pyrolysis process. Therefore, with the aid of a suitable catalyst, a higher yield and selectivity of desired yield can be attained in a shorter co-pyrolysis time [143]. The advantage of introduction of bifunctional HZSM-5/LS catalyst in co-pyrolysis can be observed from the DTG curves in Fig. 8(e) and 8(g) where the rate of dw/dt for both catalytic co-pyrolysis LDPE/MA and HDPE/MA have decreased significantly as compared to non-catalytic co-pyrolysis process, indicating that lesser energy required in the degradation process. The DTG_{max} has reduced from 74.71–138.16 wt%/min (non-catalytic co-pyrolysis) to 51.52–84.12 wt%/min (catalytic co-pyrolysis). This proved that with the presence of catalyst, the rate of decomposition of the mixtures were faster with a lower degradation rate loss, by speeding up the reactions as well as enhancing rate of degradation through the $c-c/c-o$ cleavage, [144–146].

3.3. Kinetic and thermodynamic analysis

Based on the estimated E_s and A values from simplified DAEM *via* plotting of Arrhenius plot of $ln\left(\frac{\beta}{T^2}\right)$ against $\frac{1}{T}$, G-DAEM (following the iteration method of the values of E_s and A using MATLAB R2019b by taking the initial guess values obtained from simplified DAEM, [125]), the standard deviation (σ), maximum activation energy (E_{max}) and A values attained in this study were in the range of 5–70 kJ/mol, 50–350 kJ/mol and 10^4–10^{30} s^{-1}, respectively. The average σ value can be obtained from the *f(E)* distribution curves of G-DAEM (Fig. S 2 (a)–(e)) at peak value of *f(E)*~0.0114. The value of σ represents the difference from the mean or expected value. Lower σ values suggest that most of the numbers were close to the mean, while higher σ values indicate that the numbers were further apart from the mean which leads to a wider distribution curve. Therefore, the mean values for σ

Table 6
Weight loss of thermal decomposition for catalytic and non-catalytic pyrolysis of MA with polyethylene blends at different heating rate.

Samples	Heating rate (β, K/min)	T_0 (K)	T_f (K)	T_p (K)	Weight loss (wt%)	-DTG$_{max}$ (wt%/min)	Fit (%)
Pure MA (Stage II)	10	456	824	521	50.930	2.20	3.56
	20	458	825	524	54.892	4.34	5.74
	30	459	826	531	54.742	6.39	8.81
	50	460	827	537	53.760	10.23	11.62
	100	463	829	542	53.778	21.11	10.58
	Average	–	–	531	53.620	–	8.06
Pure LDPE (Stage II)	10	529	800	681	63.523	12.25	9.90
	20	539	808	707	69.041	30.33	4.18
	30	541	820	722	49.575	41.49	5.89
	50	545	825	741	76.267	57.50	13.99
	100	559	827	768	77.312	145.01	9.38
	Average	–	–	724	67.144	–	8.67
LDPE + MA (Stage II)	10	475	803	675	61.227	14.31	7.27
	20	477	813	672	45.395	16.32	7.30
	30	483	830	669	48.017	18.50	8.73
	50	485	831	716	39.992	30.57	8.20
	100	490	841	764	43.236	74.71	9.22
	Average	–	–	699	47.573	–	8.14
Pure HDPE (Stage II)	10	480	747	741	60.616	18.03	8.40
	20	518	767	729	60.975	21.64	9.76
	30	519	775	772	55.420	52.03	8.71
	50	520	814	767	54.702	66.87	8.82
	100	525	859	779	50.188	128.16	7.19
	Average	–	–	757	56.380	–	8.58
HDPE + MA (Stage II)	10	483	815	734	63.220	12.61	7.81
	20	486	826	756	62.057	22.29	9.40
	30	488	862	759	45.718	21.88	8.03
	50	488	878	770	57.829	53.57	8.60
	100	497	880	790	72.064	86.40	7.14
	Average	–	–	762	60.178	–	8.20
LDPE + MA + HZSM-5/LS (Stage II)	10	473	777	700	60.565	24.55	7.79
	20	474	810	692	66.009	23.64	8.16
	30	478	813	707	56.845	23.21	7.76
	50	478	830	735	65.973	35.81	6.87
	100	484	831	735	41.897	51.52	13.67
	Average	–	–	714	58.258	–	8.85
HDPE + MA + HZSM-5/LS (Stage II)	10	481	799	741	60.681	10.11	6.93
	20	485	809	706	65.368	20.11	8.76
	30	485	818	761	57.436	30.30	8.50
	50	487	840	756	55.339	33.49	8.61
	100	489	876	789	66.266	84.12	7.41
	Average	–	–	754	61.018	–	8.04

Note: T_0 = Initial temperature of stage II; T_f = Final temperature of stage II; T_p = Peak temperature of stage I.

and E_{max} were chosen as 35 kJ/mol and 200 kJ/mol while the A was taken from the results of simplified DAEM. For simplified DAEM, the validity of the model was determined by the values of R^2, whereas for G-DAEM, a fit percentage was calculated by Eq. 35 (shown in Electronic Supplementary) using MATLAB R2019b to verify the error of the model.

Fig. 9(a)–(e) illustrate the Arrhenius plot of $ln\left(\frac{\beta}{T^2}\right)$ against $\frac{1}{T}$ derived from simplified DAEM model at selected $\frac{V}{V^*}$ ranging from 0.1–0.9. Most of the plots were non-linear and hence, line fitting was performed and the values of coefficient of determination (R^2) were determined. The R^2 value indicates the linear regression of the chosen model with the linear fitting line, where a positive value of R^2 near to 1 is more favorable in term of precision. From the overall DTG results, the values of R^2 determined were ranging from 0.9–0.99 which indicates that the chosen model does fitted well. All of the values for kinetic and thermodynamic analyses were tabulated as shown in Table 7 and Table 8, respectively. The estimated mean E_s values using simplified DAEM for individual pyrolysis of pure samples of MA, LDPE and HDPE are 135 kJ/mol, 89 kJ/mol and 104 kJ/mol, respectively. Meanwhile, the estimated mean *Es* values using simplified DAEM for co-pyrolysis of MA and LDPE and co-pyrolysis of MA and HDPE are 104.3 kJ/mol and 119.2 kJ/mol, respectively. In another words, the estimated mean *Es* values for co-pyrolysis of MA and LDPE is slightly lower compared to co-pyrolysis of MA and HDPE. It was also found that pure MA requires much higher energy (*ca.* 31–46 kJ/mol) during its pyrolysis process as compared to pure polyethylene, mainly attributed to the structural complexity of pure MA consisting a complex mixture of cellulose, hemicellulose, lignin, proteins, carbohydrates and lipids. Conversely, pure polyethylene is made up of simple polymer chains. Thus, pure MA tends to have a higher E_s values over pure polyethylene. However, after introducing pure polyethylene blends into the pure MA, the E_s value was reduced, indicating that there was a positive synergistic effect in reduction of thermal degradation rate between the blends. For instance, the E_s value of pure MA decreased to 107 kJ/mol after blending with LDPE. Correspondingly, in co-pyrolysis of HDPE and MA, the E_s has been reduced to a value of 119 kJ/mol. This finding revealed the E_s value has reduced in co-pyrolysis of LDPE with pure MA or HDPE with pure MA mixture compared to the individual pure MA. In addition, a higher E_s was shown in the HDPE degradation plot as compared to LDPE due to a stronger tensile strength between molecules and density in HDPE. Therefore, more energy was needed to break down the HDPE intermolecular bonds for degradation as discussed earlier [147–149]. In the case of adding small amount of HZSM-5/LS catalyst, the *Es* for co-pyrolysis of HDPE and MA and LDPE and MA mixtures have reduced ~10%, which is in good agreement with the DTG$_{max}$ reported earlier.

Comparing with the G-DAEM model, the values of E_s for every sample were very much closer to those estimated by simplified DAEM

Table 7
Summary of activation energies and pre-exponential values at respective conversion (α) for non-catalytic and catalytic co-pyrolysis of MA with PE Blends.

Samples	α	Kinetic models							
		DAEM				Gaussian-DAEM			
		E_S (kJ/mol)	A (min^{-1})	R^2	Fitted Equation	E_S (kJ/mol)	A (nin^{-1})	F(E)	σ
Pure MA (Stage II)	0.1	124	7.911×10^{12}	0.9945	$-1.490\times10^{4}x + 20.697$	125	7.91×10^{12}		
	0.2	110	5.892×10^{10}	0.9949	$-1.328\times10^{4}x + 15.913$	112	5.89×10^{10}		
	0.3	113	3.327×10^{10}	0.9939	$-1.361\times10^{4}x + 15.317$	113	3.33×10^{10}		
	0.4	119	3.601×10^{10}	0.9853	$-1.436\times10^{4}x + 15.342$	120	3.60×10^{10}		
	0.5	118	7.817×10^{9}	0.9810	$-1.424\times10^{4}x + 13.824$	119	7.82×10^{9}	0.0114	34.98
	0.6	120	3.662×10^{9}	0.9773	$-1.448\times10^{4}x + 13.048$	121	3.66×10^{9}		
	0.7	131	7.681×10^{9}	0.9684	$-1.571\times10^{4}x + 13.707$	131	7.68×10^{9}		
	0.8	163	6.186×10^{11}	0.9787	$-1.966\times10^{4}x + 17.872$	164	6.19×10^{11}		
	0.9	212	3.143×10^{14}	0.9581	$-2.551\times10^{4}x + 23.842$	212	3.14×10^{14}		
	Average	134.4	3.588×10^{13}	0.9813	–	135.2	3.59×10^{13}		
Pure LDPE (Stage II)	0.1	88	3.708×10^{7}	0.9707	$-1.062\times10^{4}x + 8.766$	88	3.71×10^{7}		
	0.2	90	1.574×10^{7}	0.9937	$-1.088\times10^{4}x + 7.885$	91	1.57×10^{7}		
	0.3	94	4.160×10^{6}	0.9912	$-1.135\times10^{4}x + 6.512$	94	4.16×10^{6}		
	0.4	93	2.043×10^{6}	0.9821	$-1.114\times10^{4}x + 5.820$	93	2.04×10^{6}		
	0.5	89	8.878×10^{5}	0.9761	$-1.074\times10^{4}x + 5.023$	90	8.88×10^{5}	0.0114	34.99
	0.6	85	3.617×10^{5}	0.9864	$-1.026\times10^{4}x + 4.170$	86	3.62×10^{5}		
	0.7	77	7.357×10^{4}	0.9909	$-9.278\times10^{3}x + 2.678$	77	7.36×10^{4}		
	0.8	88	4.249×10^{5}	0.9938	$-1.062\times10^{4}x + 4.297$	89	4.25×10^{5}		
	0.9	94	9.059×10^{5}	0.9301	$-1.129\times10^{4}x + 4.993$	93	9.06×10^{5}		
	Average	88.7	6.853×10^{6}	0.9794	–	89	6.85×10^{6}		
LDPE + MA (Stage II)	0.1	96	4.353×10^{8}	0.9199	$-1.159\times10^{4}x + 11.141$	97	4.35×10^{8}		
	0.2	90	1.443×10^{7}	0.9315	$-1.080\times10^{4}x + 7.805$	90	1.44×10^{7}		
	0.3	100	2.789×10^{7}	0.9119	$-1.200\times10^{4}x + 8.359$	100	2.79×10^{7}		
	0.4	105	3.549×10^{7}	0.8987	$-1.258\times10^{4}x + 8.552$	104	3.55×10^{7}		
	0.5	100	1.161×10^{7}	0.9188	$-1.209\times10^{4}x + 7.475$	105	1.16×10^{7}	0.0114	34.99
	0.6	91	1.480×10^{6}	0.9250	$-1.093\times10^{4}x + 5.516$	91	1.48×10^{6}		
	0.7	95	2.127×10^{6}	0.9324	$-1.143\times10^{4}x + 5.834$	96	2.13×10^{6}		
	0.8	104	6.219×10^{6}	0.9214	$-1.257\times10^{4}x + 6.812$	104	6.22×10^{6}		
	0.9	151	4.187×10^{9}	0.9103	$-1.817\times10^{4}x + 12.955$	152	4.19×10^{9}		
	Average	103.6	5.246×10^{8}	0.9189	–	104.3	5.25×10^{8}		
LDPE + MA + HZSM-5/LS (Stage II)	0.1	112	1.479×10^{11}	0.9832	$-1.353\times10^{4}x + 16.815$	113	1.48×10^{11}		
	0.2	91	2.390×10^{8}	0.9073	$-1.091\times10^{4}x + 10.602$	91	2.39×10^{8}		
	0.3	89	6.820×10^{7}	0.8933	$-1.065\times10^{4}x + 9.372$	88	6.82×10^{7}		
	0.4	87	2.944×10^{7}	0.9165	$-1.049\times10^{4}x + 8.547$	88	2.94×10^{7}		
	0.5	88	1.895×10^{7}	0.9725	$-1.056\times10^{4}x + 8.100$	87	1.89×10^{7}	0.0114	34.99
	0.6	94	3.936×10^{7}	0.9722	$-1.131\times10^{4}x + 8.763$	94	3.94×10^{7}		
	0.7	99	5.910×10^{7}	0.9374	$-1.187\times10^{4}x + 9.120$	98	5.91×10^{7}		
	0.8	95	1.667×10^{7}	0.9171	$-1.143\times10^{4}x + 7.893$	95	1.67×10^{7}		
	0.9	102	4.252×10^{7}	0.8952	$-1.236\times10^{4}x + 8.751$	103	4.25×10^{7}		
	Average	95.2	1.649×10^{10}	0.9327	–	95.2	1.65×10^{10}		
Pure HDPE (Stage II)	0.1	91	7.092×10^{6}	0.9426	$-1.089\times10^{4}x + 7.086$	91.00	7.09×10^{6}		
	0.2	87	1.110×10^{6}	0.9697	$-1.044\times10^{4}x + 5.274$	87.00	1.11×10^{6}	0.0114	34.99
	0.3	83	1.403×10^{5}	0.9921	$-9.939\times10^{3}x + 3.255$	83	1.32×10^{5}		
	0.4	82	1.948×10^{5}	0.9930	$-9.806\times10^{3}x + 3.597$	81	1.95×10^{5}		
	0.5	88	3.805×10^{5}	0.9928	$-1.057\times10^{4}x + 4.191$	88	3.81×10^{5}		
	0.6	88	3.387×10^{5}	0.9949	$-1.062\times10^{4}x + 4.069$	89	3.39×10^{5}		
	0.7	90	3.559×10^{5}	0.9937	$-1.077\times10^{4}x + 4.105$	90	3.56×10^{5}		
	0.8	95	6.736×10^{5}	0.9874	$-1.144\times10^{4}x + 4.683$	95	6.74×10^{5}		
	0.9	111	6.688×10^{6}	0.9878	$-1.330\times10^{4}x + 6.828$	111	6.69×10^{6}		
	Average	90.6	1.885×10^{6}	0.9838	–	90.6	1.89×10^{6}		
HDPE + MA (Stage II)	0.1	167	1.644×10^{12}	0.9897	$-2.007\times10^{4}x + 18.829$	167	1.64×10^{12}		
	0.2	140	5.409×10^{9}	0.9543	$-1.682\times10^{4}x + 13.289$	139	5.41×10^{9}		
	0.3	120	1.213×10^{8}	0.9171	$-1.440\times10^{4}x + 9.646$	119	1.21×10^{8}	0.0114	35.00
	0.4	109	1.505×10^{7}	0.8954	$-1.307\times10^{4}x + 7.657$	109	1.50×10^{7}		
	0.5	110	1.172×10^{7}	0.9338	$-1.317\times10^{4}x + 7.399$	110	1.17×10^{7}		
	0.6	105	3.686×10^{6}	0.9699	$-1.262\times10^{4}x + 6.285$	105	3.69×10^{6}		
	0.7	105	3.039×10^{6}	0.9977	$-1.267\times10^{4}x + 6.087$	105	3.04×10^{6}		
	0.8	104	2.312×10^{6}	0.9968	$-1.252\times10^{4}x + 5.826$	104	2.31×10^{6}		
	0.9	115	1.078×10^{7}	0.9911	$-1.383\times10^{4}x + 7.266$	115	1.08×10^{7}		
	Average	119.4	1.833×10^{11}	0.9606	–	119.2	1.83×10^{11}		
HDPE + MA + HZSM-5/LS (Stage II)	0.1	189	9.985×10^{13}	0.8928	$-2.278\times10^{4}x + 22.808$	189	9.98×10^{13}		
	0.2	117	1.067×10^{8}	0.9757	$-1.404\times10^{4}x + 9.543$	116	1.07×10^{8}	0.0114	35.00
	0.3	95	1.891×10^{6}	0.9782	$-1.147\times10^{4}x + 5.712$	96	1.89×10^{6}		
	0.4	83	1.642×10^{5}	0.9577	$-9.935\times10^{3}x + 3.413$	83	1.64×10^{5}		
	0.5	85	1.942×10^{5}	0.9332	$-1.021\times10^{4}x + 3.553$	85	1.94×10^{5}		
	0.6	87	2.143×10^{5}	0.9290	$-1.041\times10^{4}x + 3.632$	87	2.14×10^{5}		
	0.7	91	3.825×10^{5}	0.9519	$-1.099\times10^{4}x + 4.157$	91	3.82×10^{5}		
	0.8	105	2.851×10^{6}	0.9664	$-1.265\times10^{4}x + 6.026$	105	2.85×10^{6}		
	0.9	126	5.315×10^{7}	0.8609	$-1.514\times10^{4}x + 8.771$	126	5.31×10^{7}		
	Average	108.7	1.109×10^{13}	0.9384	–	108.7	1.11×10^{13}		

Table 8
Summary of Thermodynamic Parameters at Respective Conversion (α) for non-catalytic and catalytic co-pyrolysis of MA with PE blends.

Samples	α	Kinetic models					
		DAEM			Gaussian-DAEM		
		ΔH(J/mol)	ΔG (J/mol)	ΔS (J/mol K)	ΔH(J/mol)	ΔG (J/mol)	ΔS (J/mol K)
Pure MA (Stage II)	0.1	1.195×10^5	1.254×10^5	−11.172	1.21×10^5	1.27×10^5	−11.17
	0.2	1.056×10^5	1.356×10^5	−56.499	1.07×10^5	1.37×10^5	−56.50
	0.3	1.082×10^5	1.426×10^5	−64.759	1.08×10^5	1.42×10^5	−64.76
	0.4	1.142×10^5	1.499×10^5	−67.129	1.15×10^5	1.50×10^5	−67.13
	0.5	1.129×10^5	1.592×10^5	−87.254	1.14×10^5	1.60×10^5	−87.25
	0.6	1.146×10^5	1.679×10^5	−100.269	1.15×10^5	1.68×10^5	−100.27
	0.7	1.247×10^5	1.760×10^5	−96.758	1.25×10^5	1.76×10^5	−96.76
	0.8	1.572×10^5	1.837×10^5	−50.009	1.58×10^5	1.84×10^5	−50.01
	0.9	2.055×10^5	1.927×10^5	24.168	2.05×10^5	1.93×10^5	24.17
	Average	1.292×10^5	1.592×10^5	−56.631	1.30×10^5	1.60×10^5	−56.63
Pure LDPE (Stage II)	0.1	8.248×10^4	1.631×10^5	−111.437	8.22×10^4	1.63×10^5	−111.44
	0.2	8.414×10^4	1.775×10^5	−129.053	8.47×10^4	1.78×10^5	−129.05
	0.3	8.767×10^4	1.957×10^5	−149.305	8.73×10^4	1.95×10^5	−149.31
	0.4	8.559×10^4	2.045×10^5	−164.320	8.60×10^4	2.05×10^5	−164.32
	0.5	8.199×10^4	2.118×10^5	−179.337	8.27×10^4	2.13×10^5	−179.34
	0.6	7.775×10^4	2.201×10^5	−196.712	7.84×10^4	2.21×10^5	−196.71
	0.7	6.864×10^4	2.427×10^5	−240.576	6.85×10^4	2.43×10^5	−240.58
	0.8	8.058×10^4	2.243×10^5	−198.615	8.13×10^4	2.25×10^5	−198.62
	0.9	8.625×10^4	2.218×10^5	−187.262	8.54×10^4	2.21×10^5	−187.26
	Average	8.168×10^4	2.068×10^5	−172.957	8.18×10^4	2.07×10^5	−172.96
LDPE + MA (Stage II)	0.1	9.133×10^4	1.484×10^5	−81.707	9.19×10^4	1.49×10^5	−81.71
	0.2	8.409×10^4	1.686×10^5	−120.992	8.43×10^4	1.69×10^5	−120.99
	0.3	9.352×10^4	1.820×10^5	−126.546	9.38×10^4	1.82×10^5	−126.55
	0.4	9.811×10^4	1.889×10^5	−129.943	9.75×10^4	1.88×10^5	−129.94
	0.5	9.384×10^4	1.948×10^5	−144.457	9.83×10^4	1.99×10^5	−144.46
	0.6	8.381×10^4	2.060×10^5	−174.832	8.39×10^4	2.06×10^5	−174.83
	0.7	8.787×10^4	2.097×10^5	−174.381	8.88×10^4	2.11×10^5	−174.38
	0.8	9.717×10^4	2.135×10^5	−166.383	9.67×10^4	2.13×10^5	−166.38
	0.9	1.441×10^5	2.090×10^5	−92.898	1.45×10^5	2.10×10^5	−92.90
	Average	9.709×10^4	1.912×10^5	−134.682	9.78×10^4	1.92×10^5	−134.68
LDPE + MA + HZSM-5/LS (Stage II)	0.1	1.078×10^5	1.330×10^5	−35.298	1.08×10^5	1.34×10^5	−35.30
	0.2	8.561×10^4	1.460×10^5	−84.646	8.59×10^4	1.46×10^5	−84.65
	0.3	8.325×10^4	1.534×10^5	−98.200	8.27×10^4	1.53×10^5	−98.20
	0.4	8.164×10^4	1.601×10^5	−109.967	8.24×10^4	1.61×10^5	−109.97
	0.5	8.193×10^4	1.676×10^5	−120.017	8.11×10^4	1.67×10^5	−120.02
	0.6	8.766×10^4	1.759×10^5	−123.565	8.77×10^4	1.76×10^5	−123.57
	0.7	9.224×10^4	1.799×10^5	−122.738	9.15×10^4	1.79×10^5	−122.74
	0.8	8.795×10^4	1.930×10^5	−147.202	8.79×10^4	1.93×10^5	−147.20
	0.9	9.556×10^4	1.955×10^5	−139.935	9.58×10^4	1.96×10^5	−139.93
	Average	8.929×10^4	1.671×10^5	−109.063	8.93×10^4	1.67×10^5	−109.06
Pure HDPE (Stage II)	0.1	8.456×10^4	1.777×10^5	−123.018	8.50×10^4	1.78×10^5	−123.02
	0.2	8.017×10^4	1.958×10^5	−152.670	8.04×10^4	1.96×10^5	−152.67
	0.3	7.546×10^4	2.167×10^5	−186.456	7.58×10^4	2.17×10^5	−186.46
	0.4	7.393×10^4	2.214×10^5	−194.707	7.34×10^4	2.21×10^5	−194.71
	0.5	8.019×10^4	2.239×10^5	−189.794	8.03×10^4	2.24×10^5	−189.79
	0.6	8.027×10^4	2.326×10^5	−201.139	8.09×10^4	2.33×10^5	−201.14
	0.7	8.143×10^4	2.345×10^5	−202.189	8.19×10^4	2.35×10^5	−202.19
	0.8	8.696×10^4	2.361×10^5	−196.937	8.68×10^4	2.36×10^5	−196.94
	0.9	1.028×10^5	2.253×10^5	−161.756	1.03×10^5	2.26×10^5	−161.76
	Average	8.231×10^4	2.177×10^5	−178.806	8.25×10^4	2.18×10^5	−178.81
HDPE + MA (Stage II)	0.1	1.605×10^5	1.811×10^5	−26.935	1.61×10^5	1.81×10^5	−26.94
	0.2	1.332×10^5	1.929×10^5	−78.340	1.32×10^5	1.92×10^5	−78.34
	0.3	1.130×10^5	1.999×10^5	−114.083	1.12×10^5	1.99×10^5	−114.08
	0.4	1.019×10^5	2.030×10^5	−132.770	1.02×10^5	2.03×10^5	−132.77
	0.5	1.025×10^5	2.092×10^5	−140.010	1.03×10^5	2.10×10^5	−140.01
	0.6	9.753×10^4	2.190×10^5	−159.431	9.76×10^4	2.19×10^5	−159.43
	0.7	9.748×10^4	2.292×10^5	−172.859	9.71×10^4	2.29×10^5	−172.86
	0.8	9.615×10^4	2.314×10^5	−177.514	9.60×10^4	2.31×10^5	−177.51
	0.9	1.075×10^5	2.228×10^5	−151.455	1.07×10^5	2.23×10^5	−151.46
	Average	1.122×10^5	2.098×10^5	−128.155	1.12×10^5	2.10×10^5	−128.16
HDPE + MA + HZSM-5/LS (Stage II)	0.1	1.833×10^5	1.780×10^5	7.117	1.83×10^5	1.78×10^5	7.12
	0.2	1.101×10^5	1.963×10^5	−114.865	1.09×10^5	1.96×10^5	−114.86
	0.3	8.824×10^4	2.105×10^5	−162.944	8.88×10^4	2.11×10^5	−162.94
	0.4	7.452×10^4	2.331×10^5	−211.251	7.49×10^4	2.33×10^5	−211.25
	0.5	7.672×10^4	2.352×10^5	−211.082	7.69×10^4	2.35×10^5	−211.08
	0.6	7.837×10^4	2.375×10^5	−211.998	7.88×10^4	2.38×10^5	−212.00
	0.7	8.310×10^4	2.390×10^5	−207.644	8.27×10^4	2.39×10^5	−207.64
	0.8	9.732×10^4	2.285×10^5	−174.719	9.72×10^4	2.28×10^5	−174.72
	0.9	1.186×10^5	2.192×10^5	−134.069	1.19×10^5	2.19×10^5	−134.07
	Average	1.011×10^5	2.197×10^5	−157.939	1.01×10^5	2.20×10^5	−157.94

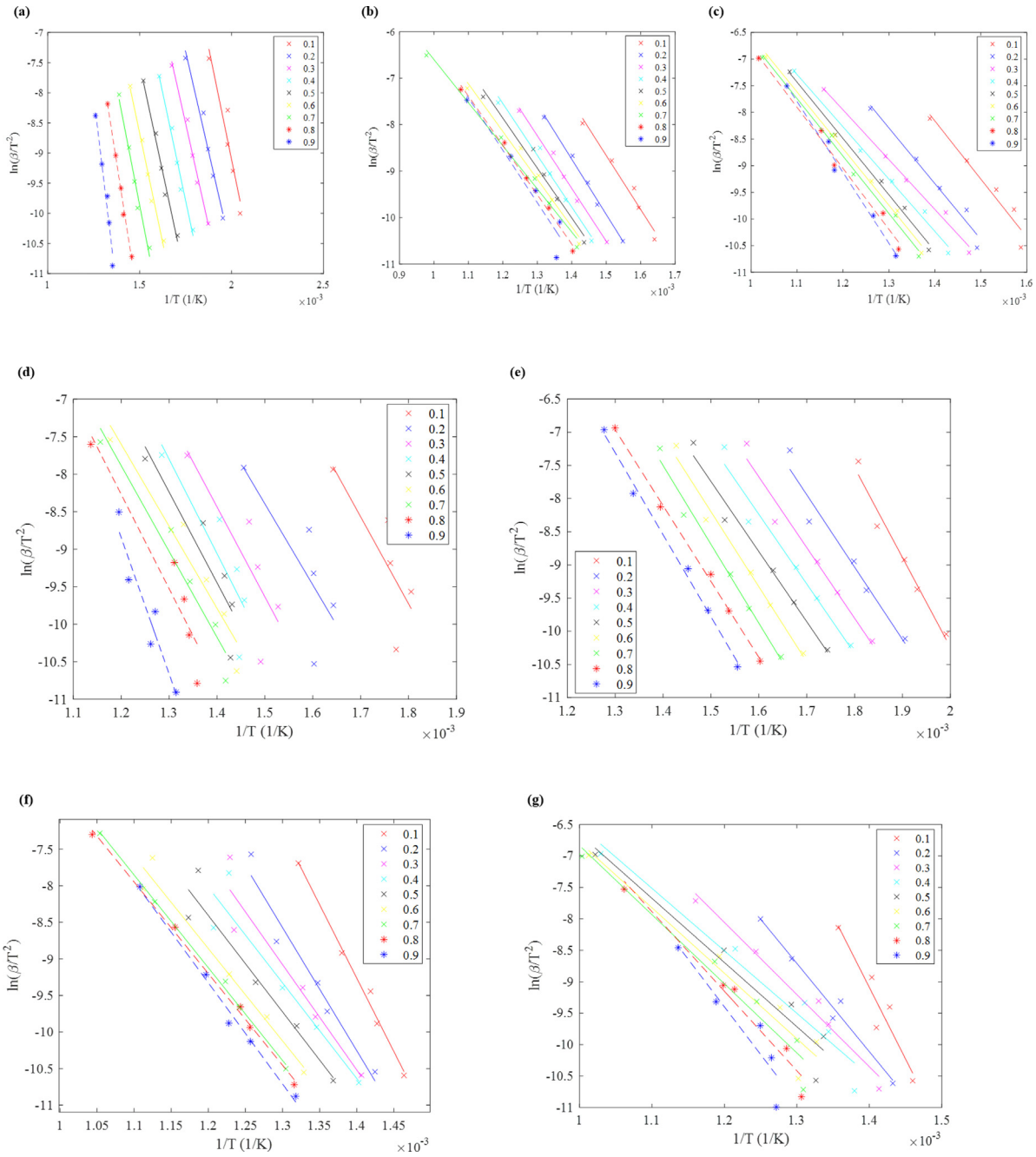

Fig. 9. Arrhenius plots of (a)–(c): non-catalytic pyrolysis of pure MA, pure LDPE and pure HDPE; (d) non-catalytic co-pyrolysis of LDPE/MA, (e) catalytic co-pyrolysis of LDPE/MA with bifunctional HZSM-5/LS catalyst, (f) non-catalytic co-pyrolysis of HDPE/MA, and (g) catalytic co-pyrolysis of HDPE/MA with bifunctional HZSM-5/LS catalyst.

model. As mentioned earlier, pure MA has the highest mean E_s value (135 kJ/mol) opposing to pure LDPE and HDPE which require lower mean E_s values (89 kJ/mol and 90.56 kJ/mol respectively). Both models have equal values of A as it was kept constant while running iterative calculations *via* G-DAEM. The results for the average A values obtained for both models were concluded as 3.588×10^{13}, 6.853×10^{6}, 1.885×10^{6}, 5.246×10^{8} and 1.833×10^{11} min^{-1} for pure MA, pure LDPE, pure HDPE, co-pyrolysis of LDPE/MA and HDPE/MA, respectively. According to the G-DAEM, the distribution curve tends to shift to the right as the E_s increased, and shift to the left when the E_s decreased. All distribution curves were having equal width as the σ was kept constant for all cases. In addition, the validity of G-DAEM was verified for each sample where the fitting percentage resembles the deviation between experimental and calculated conversion. Hence, the lower the values of fitting percentage, the higher the accuracy. The average fitting percentages were in the range of 8.06–8.85% with a deviation below 15% and thus, the results obtained in this study were tolerable.

Based on Table 8, it appeared that the overall process was endothermic as the changes in ΔH were positive values, non-spontaneous as positive changes in ΔG were obtained, and the process was less disorder as negative changes in ΔS were attained. Most importantly, the values of ΔH and ΔS were lesser in co-pyrolysis of the mixture (plastic waste and biomass) compared to pyrolysis of pure MA, concluding that the pyrolytic conversion of mixture of plastic wastes and biomass produces an activated complex with a more organized structure (i.e., a state near to its thermodynamic equilibrium) than that of the initial reactants (*Chlorella vulgaris*). On the other hand, the ΔG values reduced in co-pyrolysis of MA/LDPE or HDPE blends. This can be explained through the non-spontaneity process, suggesting that the energy absorbed in the pyrolysis system behaves endothermically during the decomposition of

Table 9
Optimized reaction conditions of co-pyrolysis of microalgae and plastic wastes mixture for different temperature ranges.

Temperature range (K)	HDPE fraction	LDPE fraction	MA fraction	Catalyst required	Heating rate (K/min)	Reactor temperature (K)	Conversion (%)
303.15–323.15	0.00	0.02	0.98	True	14	323.15	4.3
323.15–373.15	0.02	0.19	0.79	True	28	373.15	5.3
373.15–473.15	0.03	0.04	0.93	True	44	473.15	14.1
473.15–573.15	0.06	0.20	0.74	False	12	573.15	26.2
573.15–673.15	0.03	0.22	0.76	False	22	673.15	40.2
673.15–773.15	0.18	0.75	0.06	False	20	773.15	97.4
773.15–873.15	0.59	0.17	0.24	True	38	873.15	99.0
873.15–973.15	0.68	0.28	0.03	True	50	973.15	99.6
973.15–1073.15	0.44	0.53	0.03	True	72	1073.15	99.6
1073.15–1173.15	0.13	0.77	0.11	True	82	1173.15	99.6

samples. [150–152]. The thermodynamic features illustrated that the co-pyrolysis of plastic waste and biomass could be a good combination for pyrolysis and that its bioenergy valorization is an alternative for plastic waste management, promoting sustainability as part of a circular economy.

3.4. Optimization of the conversion rate via neuro-evolution

Based on Fig. 10(b-e), it can be observed that the errors (MAE, RMSE, MBE) and R^2 for both training and validation were the highest when a shallow neural network (with depth=1) was used when compared to a deep neural network. This suggests that the TGA data has a high non-linearity that should be modeled using deep neural networks. For all the validation indicators, the depth with the lowest training errors (MAE=0.00318, RMSE=0.00736, MBE=0.00018), lowest validation errors (MAE=0.00259, RMSE=0.00637, MBE=0.00073) and high R^2 (Training R^2 = 0.99962, Validation R^2 = 0.99971) was the ANN with depth of 6. This optimal ANN model has neural architecture of "133, 245, 440, 203, 477, 1", activation function of "elu, hard sigmoid, sigmoid, sigmoid, hard sigmoid, sigmoid". Using a separate test set (Fig. 10(f)), the optimal ANN model obtained very similar error metrics and R^2 values. This shows that the ANN was not overfitted to only the training data and the model does not have a significant bias due to its low MBE observed in all training, validation, and test sets.

Fig. 11(a) visually explains the mass fraction constraints that were implemented during the simulated annealing optimization procedure for reaction condition optimization. The mass of reactants is separated from the mass of the catalyst using mass fraction. From Fig. 11(b), the inclusion of microalgae at lower mass fractions of HDPE enhanced the mixed conversion of the thermal reaction, increasing the reaction mass conversion. This effect was also valid when microalgae were added into LDPE (Fig. 11(c)), however, a smaller microalgae mass fraction was required for enhanced reaction conversion. Based on the findings, the catalyst has the smallest effects on the MA conversion (Fig. 11(d)), however this effect was not having significant evident throughout all ranges of mass fraction. This also indicates that the use of the catalyst for this reaction has to be further studied using reaction condition optimization to ensure optimal usage. In Fig. 11(e), there was a clear effect of MA mass fraction on the optimal heating rate which produces higher reaction conversion.

An indication of variable effects can be deduced from Fig. 11(b-e), however, the optimum conditions were difficult to be determined from such snapshots (contour plots) of multidimensional reaction models. To obtain the optimal reaction conditions, these multivariate variables were optimized subsequently using simulated annealing optimization to maximize the reaction conversion (Table 9). It can be observed that the conversion was very low (≤14.1%) at temperatures below 473 K and the reaction conversion increased up to 97.4% when the reactor temperature was 773 K. In general, the optimal heating rate increases with reactor temperature, however it is also affected by the fractions of reactant, suggesting that the heat capacity of the reactants and the degradation were higher due to a more effective heat transfer between the reactant molecules. This shows that the true effective range of the catalyst degradation was at a temperature of 873 K and above. This is also in agreement with our previous work [26], which found that HZSM-based catalysts operate more effectively at high temperatures for microalgae reactants. Furthermore, mixing of HDPE, LDPE and microalgae reactants show a positive synergistic effect on the thermal degradation rate, as commonly (except under temperature range between 303.15–323.15 K) all three reactants are required to obtain optimal performance. However, at lower temperatures (<673.15 K), HDPE was only required at a small amount ~0.10 mg in the mix. Vice-versa, while at higher temperatures (>873.15 K), MA was only required in small fractions ~0.10 mg to achieve optimal conversion. This phenomenon can be explained through MA structure, where long chain protein and carbohydrate take longer reaction time to be break down. Also, the ΔS of pure MA attained was much higher than LDPE and HDPE, and thus, the activated complex is in a less "organized" structure and lower availability for the energy's system energy to generate biofuel [21]. Based on the PDSE-ANN model, the predicted optimum pyrolysis conditions were a tri-combination of LDPE (0.13%) + HDPE (0.77%) + MA (0.11%) with the aid of HZSM-5/LS catalyst at 1173.15 K and 82 K/min to yield a 99.6% thermal degradation rate. In order to determine the reliability and accuracy of the model, 3 experimental runs were repeated using the predicted optimum conditions. Notably, the thermal degradation rate (96.7%, 98.2% and 97.8%) attained was very close to the one predicted, suggesting that neural network model exhibits a good optimization modeling prediction ability.

4. Conclusion

This paper concludes by highlighting its objective, which aimed to contribute to the understanding of the synergistic effect of co-pyrolysis of microalgae with plastic wastes. The study progressed through various steps, including reviewing recent work on the pyrolysis characteristics of microalgae and plastic waste, selecting suitable feedstock for co-pyrolysis process, evaluating iso-conversional kinetic models, choosing the most precise kinetic models, identifying kinetic and thermodynamic parameters, and ultimately determining the optimum thermal conversion rate through a neuro-evolutionary approach. Together, these stages improve our understanding of the co-pyrolysis process and offer valuable insights for future research in this field. The E_s and A with first reaction order were obtained from two iso-conversational kinetic models, namely simplified distributed activation energy model (DAEM) and Gaussian distributed activation energy model (G-DAEM), whereas the change of enthalpy, entropy and Gibbs free energy were determined from the activation energy values obtained from the kinetic analysis. The co-pyrolysis of biomass and plastic demonstrated positive synergistic effect as compared to pyrolysis of a pure component. From the thermodynamic aspects, the overall co-pyrolysis process was found to be endothermic, non-spontaneous and less disorder. Also, the optimization of the co-pyrolysis process *via* neural network PDSE algorithm with subsequent simulated annealing suggests that the optimal reaction conditions were pyrolyzing a tri-combination of LDPE (0.13%) + HDPE (0.77%) + MA (0.11%) with the aid of HZSM-5/LS catalyst at

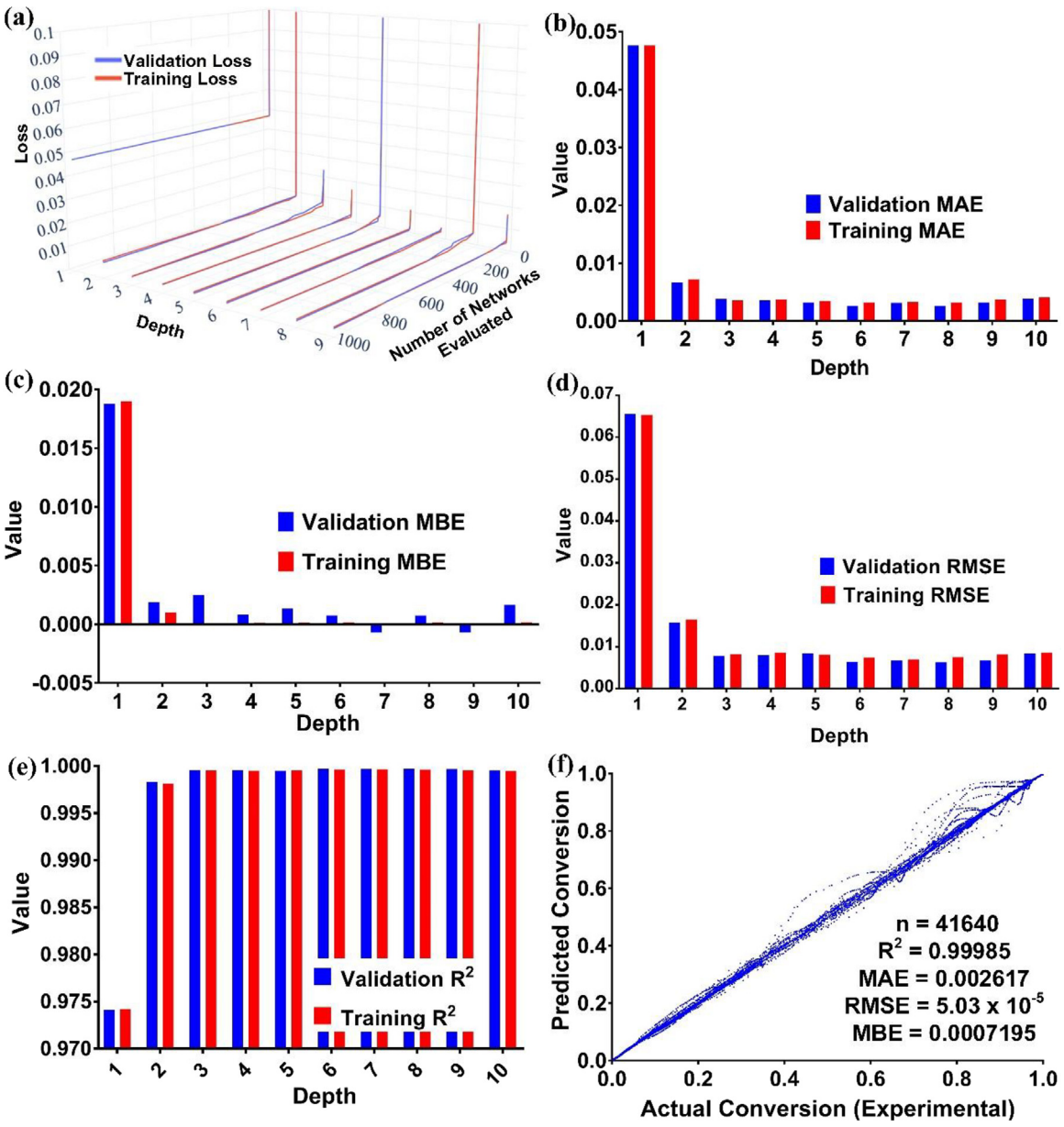

Fig. 10. (a) The effects of training loss and validation loss with respect to depth of neural network and number of networks evaluated. Training and validation metrics for the best neural network of each depth using (b) mean absolute error (c) mean bias error (d) root mean square error (e) R-square value. (f) The predicted reaction conversion against actual experimental conversion by the overall best neural network (depth=6).

1173.15 K and 82 K/min to yield a 99.6% thermal degradation rate. Most importantly, an approximate similar degradation rate of ~97.6% (average) can be obtained by repeating the TGA experiments using the predicted optimum conditions, indicating the reliability and accuracy of the neural network model. For future works, it will be promising and useful to integrate the neural network approach with kinetic and thermodynamic parameters obtained in this study to design a pilot scale co-pyrolyzer for microalgae and plastic wastes (HDPE/LDPE).

CRediT authorship contribution statement

Isabel Jia Yen Tan: Writing – original draft, Software, Investigation, Formal analysis. **Adrian Chun Minh Loy:** Writing – review & editing, Writing – original draft, Methodology, Investigation, Formal analysis. **Bridgid Lai Fui Chin:** Writing – review & editing, Visualization, Supervision, Resources, Project administration, Funding acquisition, Formal analysis, Conceptualization. **Kin Wai Cheah:** Writing – review & editing, Investigation. **Sin Yong Teng:** Writing – review & editing, Software,The Progressive Depth Investigation. **Bing Shen How:** Writing – review & editing, Investigation. **Hatem Alhazmi:** Writing – review & editing, Investigation, Conceptualization. **Wei Dong Leong:** Writing – review & editing, Investigation. **Huei Yeong Lim:** Writing – review & editing, Investigation. **Man Kee Lam:** Writing – review & editing, Investigation. **Su Shiung Lam:** Writing – review & editing, Investigation.

Declaration of competing interest

The authors declare that they have no known competing financial interests or personal relationships that could have appeared to influence the work reported in this paper.

Acknowledgments

The authors like to acknowledge Curtin University Malaysia and Centre of Biofuel and Biochemical (CBBR) of Universiti Teknologi

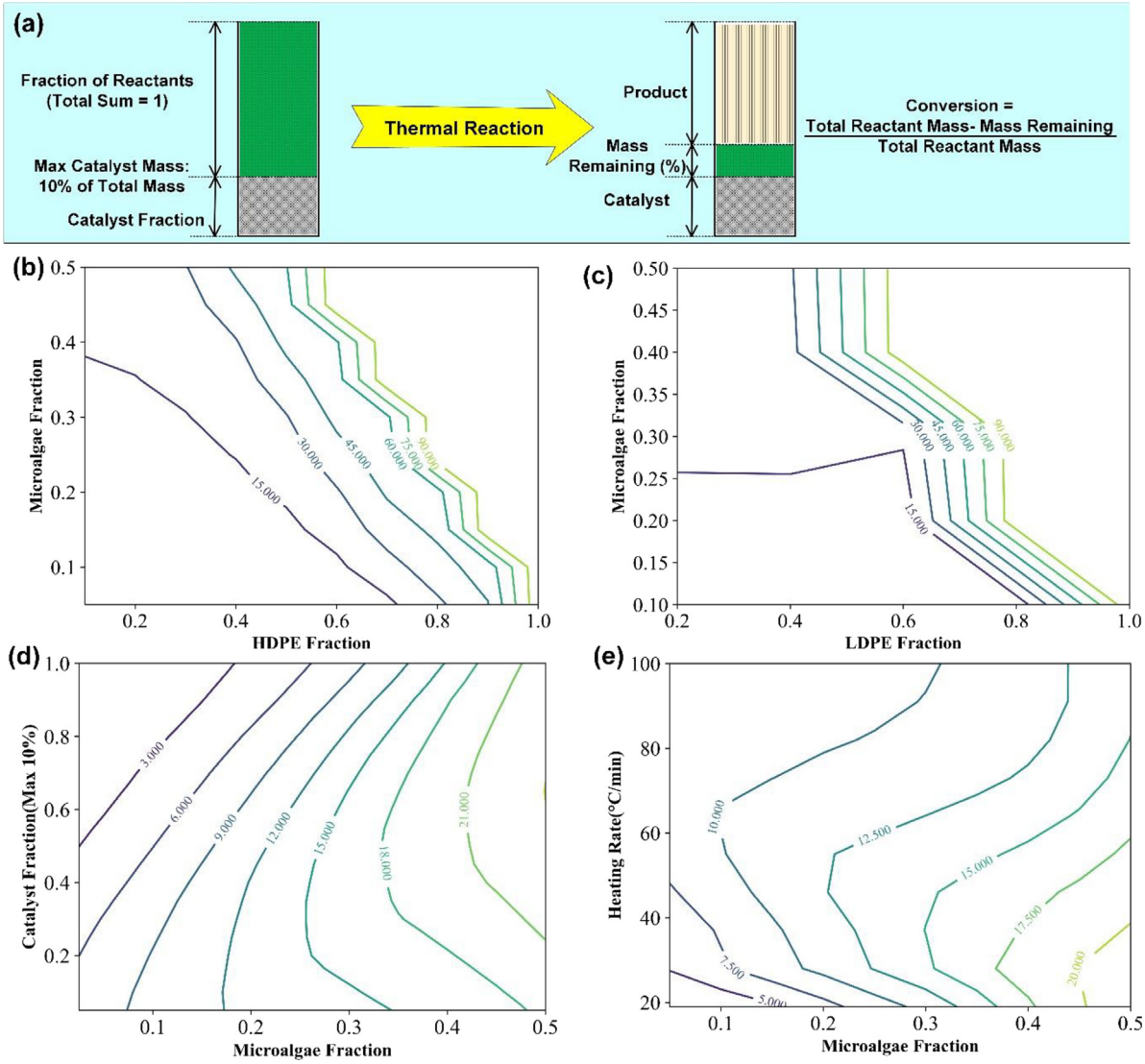

Fig. 11. (a) Visual concept of the constraints implemented during simulated annealing optimization (b) Effects of microalgae mass fraction and HDPE mass fraction on mass remaining (%) (c) Effects of microalgae mass fraction and LDPE mass fraction on mass remaining (%) (d) Effects of catalyst mass fraction and microalgae mass fraction on mass remaining (%) (e) Effects of heating rate (°C/min) and microalgae mass fraction on mass remaining (%).

PETRONAS (UTP), Malaysia for the technical support. Furthermore, financial support from Japan-ASEAN Science, Technology and Innovative Platform (JASTIP-Net). A.C.M. Loy would also like to acknowledge the "Australian Government Research Training Program" for supporting this project Lastly, How B.S. would also like to acknowledge the financial support from the Ministry of Higher Education Malaysia (MoHE) through Fundamental Research Grant Scheme (Grant number: FRGS/1/2020/TK0/SWIN/03/3). The authors would like to thank The Education University of Hong Kong for supporting Prof Lam under International Grant (UMT/CRIM/2-2/25/Jld.8 (49), Vot 53376) to perform this joint project. The research contribution from S.Y. Teng is supported by the European Union's Horizon Europe Research and Innovation Program, under Marie Skłodowska-Curie Actions grant agreement no. 101064585 (MoCEGS).

Appendix A. Supplementary data

Supplementary material related to this article can be found online at https://doi.org/10.1016/j.grets.2024.100077.

References

[1] The International Energy Agency, 2016. https://www.iea.org/newsroom/news/2016/october/iea-raises-its-five-year-renewable-growth-forecast-as-2015-marks-record-year.html. (Accessed 1 May 2018).
[2] IEA, 2020. https://www.iea.org/reports/world-energy-outlook-2020. (Accessed 17 February 2021).
[3] P. Canadell, C.L. Quéré, G. Peters, R. Andrew, R. Jackson, Carbon emissions will reach 37 billion tonnes in 2018, a record high, phys.org, 2018, https://phys.org/news/2018-12-carbon-emissions-billion-tonnes-high.html. (Accessed 2 February 2021).
[4] A. Fasolini, et al., Hydrogen from renewables: a case study of glycerol reforming, Catalysts 9 (2019) 722.
[5] World Economic Forum, Renewable infrastructure investment handbook, 2016, http://www3.weforum.org/docs/WEF_Renewable_Infrastructure_Investment_Handbook.pdf. (Accessed 11 January 2020).
[6] Z. Wang, Q. Bui, B. Zhang, The relationship between biomass energy consumption and human development: empirical evidence from BRICS countries, Energy 194 (2020) 116906.
[7] M. Bhattacharya, S. Awaworyi Churchill, S.R. Paramati, The dynamic impact of renewable energy and institutions on economic output and CO_2 emissions across regions, Renew. Energy 111 (2017) 157–167.
[8] Y.H. Chan, et al., An overview of biomass thermochemical conversion technologies in Malaysia, Sci. Total Environ. 680 (2019) 105–123.
[9] M.A. Destek, İ. Okumuş, Biomass energy consumption, economic growth and CO_2 emission in G-20 countries, Alparslan Üniversitesi Sosyal Bilimler Dergisi 7 (2019) 2149–4622.

[10] C. Sulaiman, A.S. Abdul-Rahim, C.A. Ofozor, Does wood biomass energy use reduce CO2 emissions in European Union member countries? Evidence from 27 members, J. Clean. Prod. 253 (2020) 119996.
[11] Y. Lin, et al., Thermal behavior and general distributed activation energy model kinetics of Lignite–Chinese herb residues blends during co-pyrolysis, Bioresour. Technol. 204 (2020) 122991.
[12] D.K. Park, et al., Co-pyrolysis characteristics of sawdust and coal blend in TGA and a fixed bed reactor, Bioresour. Technol. 101 (15) (2010) 6151–6156.
[13] F. Abnisa, W.M.A. Wan Daud, A review on co-pyrolysis of biomass: An optional technique to obtain a high-grade pyrolysis oil, Energy Convers. Manage. 87 (2014) 71–85.
[14] B.B. Uzoejinwa, et al., Co-pyrolysis of biomass and waste plastics as a thermochemical conversion technology for high-grade biofuel production: Recent progress and future directions elsewhere worldwide, Energy Convers. Manage. 163 (2018) 468–492.
[15] J. Cai, et al., Processing thermogravimetric analysis data for isoconversional kinetic analysis of lignocellulosic biomass pyrolysis: case study of corn stalk, Renew. Sustain. Energy Rev. 82 (2018) 2705–2715.
[16] Q. Xiong, et al., Overview of computational fluid dynamics simulation of reactor-scale biomass pyrolysis, ACS Sustain. Chem. Eng. 5 (4) (2017) 2783–2798.
[17] M. Van de Velden, et al., Fundamentals, kinetics and endothermicity of the biomass pyrolysis reaction, Renew. Energy 25 (1) (2010) 232–242.
[18] D.K.W. Gan, et al., An in-situ thermogravimetric study of pyrolysis of rice hull with alkali catalyst of $CaCO_3$, IOP Conf. Ser. Mater. Sci. Eng. 458 (2018) 012085.
[19] F. Sher, et al., Thermal and kinetic analysis of diverse biomass fuels under different reaction environment: A way forward to renewable energy sources, Energy Convers. Manage. 203 (2020) 112266.
[20] R. Barzegar, et al., TGA and kinetic study of different torrefaction conditions of wood biomass under air and oxy-fuel combustion atmospheres, J. Energy Inst. 93 (3) (2020).
[21] A.C.M. Loy, et al., Thermogravimetric kinetic modelling of in-situ catalytic pyrolytic conversion of rice husk to bioenergy using rice hull ash catalyst, Bioresour. Technol. 261 (2018) 213–222.
[22] J.T. Bong, et al., Artificial neural network approach for co-pyrolysis of *Chlorella vulgaris* and peanut shell binary mixtures using microalgae ash catalyst, Energy 207 (2020) 118289.
[23] Supriyanto, et al., Artificial neural networks model for estimating growth of polyculture microalgae in an open raceway pond, Biosyst. Eng. 177 (2019) 122–129.
[24] H. Shokrkar, S. Ebrahimi, M. Zamani, Extraction of sugars from mixed microalgae culture using enzymatic hydrolysis: Experimental study and modeling, Chem. Eng. Commun. 204 (11) (2017) 1246–1257.
[25] G. Srivastava, A.K. Paul, V.V. Goud, Optimization of non-catalytic transesterification of microalgae oil to biodiesel under supercritical methanol condition, Energy Convers. Manage. 156 (2018) 269–278.
[26] S.Y. Teng, A.C.M. Loy, W.D. Leong, B.S. How, B.L.F. Chin, V. Máša, Catalytic thermal degradation of *Chlorella vulgaris*: Evolving deep neural networks for optimization, Bioresour. Technol. 292 (2019) 121971.
[27] M. Al-Yaari, I.J. Dubdub, Application of artificial neural networks to predict the catalytic pyrolysis of HDPE using non-isothermal TGA data, Polymers 12 (2020) 1813.
[28] I. Dubdub, M. Al-Yaari, Pyrolysis of low density polyethylene: kinetic study using TGA data and ANN prediction, Polymers (Basel) 12 (4) (2020).
[29] Ö. Çepelioğullar, et al., Activation energy prediction of biomass wastes based on different neural network topologies, Fuel 220 (2018) 535–545.
[30] H. Bi, et al., Thermodynamics, kinetics, gas emissions and artificial neural network modeling of co-pyrolysis of sewage sludge and peanut shell, Fuel 284 (2021) 118988.
[31] S.P. Sathiya Prabhakaran, G. Swaminathan, V.J. Viraj, Energy conservation – A novel approach of co-combustion of paint sludge and Australian lignite by principal component analysis, response surface methodology and artificial neural network modeling, Environ. Technol. Innov. 20 (2020) 101061.
[32] S.R. Naqvi, et al., Synergistic effect on co-pyrolysis of rice husk and sewage sludge by thermal behavior, kinetics, thermodynamic parameters and artificial neural network, Waste Manage. 85 (2019) 131–140.
[33] Z. Wang, et al., Thermal degradation kinetics study of polyvinyl chloride (PVC) sheath for new and aged cables, Waste Manage. 99 (2019) 146–153.
[34] M. Buyukada, Investigation of thermal conversion characteristics and performance evaluation of co-combustion of pine sawdust and lignite coal using TGA, artificial neural network modeling and likelihood method, Bioresour. Technol. 287 (2019) 121461.
[35] T. Xie, et al., Thermal oxidative decomposition of soybean straw: Thermo-Kinetic analysis via thermogravimetric analysis and artificial neural networks, IOP Conf. Ser. Earth Environ. Sci. 581 (2020) 012019.
[36] G. Várhegyi, et al., Thermogravimetric study of biomass pyrolysis kinetics. A distributed activation energy model with prediction tests, Energy & Fuels 25 (11) (2011) 24–32.
[37] W. Kamińnski, P. Strumitto, E. Tomczak, Genetic algorithms and artificial neural networks for description of thermal deterioration processes, Drying Technol. 14 (9) (1996) 2117–2133.
[38] T. Abbas, M. Awais, F.C. Lockwood, An artificial intelligence treatment of devolatilization for pulverized coal and biomass in co-fired flames, Combust. Flame 132 (2003) 305–318.
[39] J.A. Conesa, J.A. Caballero, J.A. Reyes-Labarta, Artificial neural network for modelling thermal decompositions, J. Anal. Appl. Pyrolysis 71 (1) (2004) 343–352.
[40] T. Rasool, V.C. Srivastava, M.N.S. Khan, Utilisation of a waste biomass, walnut shells, to produce bio-products via pyrolysis: investigation using ISO-conversional and neural network methods, Biomass Convers. Biorefinery 8 (3) (2018) 647–657.
[41] S.R. Naqvi, et al., Pyrolysis of high-ash sewage sludge: Thermo-kinetic study using TGA and artificial neural networks, Fuel 233 (2018) 529–538.
[42] V.C. Liyanaarachchi, et al., Development of an artificial neural network model to simulate the growth of microalga *Chlorella vulgaris* incorporating the effect of micronutrients, J. Biotechnol. 312 (2020) 44–55.
[43] J.D.S. Castro, E.G.P. da Silva, C.F. Virgens, Evaluation of models to predict the influence of chemical pretreatment on the peels of Nephelium lappaceum L. based on pyrolysis kinetic parameters obtained using a combined Fraser-Suzuki function and Friedman's isoconversional method, J. Anal. Appl. Pyrolysis 149 (2020) 104827.
[44] J.X. J.X. Liew, et al., Synergistic effects of catalytic co-pyrolysis of corn cob and HDPE waste mixtures using weight average global process model, Renew. Energy (2021).
[45] H. Bi, et al., Pyrolysis characteristics, artificial neural network modeling and environmental impact of coal gangue and biomass by TG-FTIR, Sci. Total Environ. 751 (2021) 142293.
[46] P. Upreti, S. Ambwani, A review of third-generation biofuels from microalgae, J. Biofuels 7 (1) (2016) 14–19.
[47] G. Dragone, B. Fernandes, A.A. Vicente, J.A. Teixeira, Third generation biofuels from microalgae, 2010, https://repositorium.sdum.uminho.pt/bitstream/1822/16807/1/3067.pdf. (Accessed 20 July 2019).
[48] D.J. Gilmour, Chapter one - Microalgae for biofuel production, in: G.M. Gadd, S. Sariaslani (Eds.), Advances in Applied Microbiology, Academic Press, 2019, pp. 1–30.
[49] T.M. Mata, A.A. Martins, N.S. Caetano, Microalgae for biodiesel production and other applications: A review, Renew. Sustain. Energy Rev. 14 (1) (2010) 217–232.
[50] J. Chen, et al., The potential of microalgae in biodiesel production, Renew. Sustain. Energy Rev. 90 (2018) 336–346.
[51] X.J. Lee, et al., State of art review on conventional and advanced pyrolysis of macroalgae and microalgae for biochar, bio-oil and bio-syngas production, Energy Convers. Manage. 210 (2020) 112707.
[52] D. López-González, et al., Kinetic analysis and thermal characterization of the microalgae combustion process by thermal analysis coupled to mass spectrometry, Appl. Energy 114 (2014) 227–237.
[53] Y. Chisti, Biodiesel from microalgae, Biotechnol. Adv. 25 (3) (2007) 294–306.
[54] A.C.M. Loy, et al., Development of high microwave-absorptive bifunctional graphene oxide-based catalyst for biodiesel production, Energy Convers. Manage. 180 (2019) 1013–1025.
[55] M.K. Lam, et al., Chapter 9 - Biohydrogen production from algae, in: A. Pandey, et al. (Eds.), Biohydrogen, second ed., Elsevier, 2019, pp. 219–245.
[56] M.K. Lam, K.T. Lee, Microalgae biofuels: A critical review of issues, problems and the way forward, Biotechnol. Adv. 30 (3) (2012) 673–690.
[57] Y. Hong, et al., Kinetic study of the pyrolysis of microalgae under nitrogen and CO_2 atmosphere, Renew. Energy 145 (2020) 2159–2168.
[58] M.J.B. Fong, et al., Catalytic pyrolysis of *Chlorella vulgaris*: Kinetic and thermodynamic analysis, Bioresour. Technol. 289 (2019) 121689.
[59] H.H. Bui, K.Q. Tran, W.H. Chen, Pyrolysis of microalgae residues – A kinetic study, Bioresour. Technol. 199 (2016) 362–366.
[60] A. Agrawal, S. Chakraborty, A kinetic study of pyrolysis and combustion of microalgae *Chlorella vulgaris* using thermo-gravimetric analysis, Bioresour. Technol. 128 (2013) 72–80.
[61] K. Azizi, M. Keshavarz Moraveji, H. Abedini Najafabadi, Characteristics and kinetics study of simultaneous pyrolysis of microalgae *Chlorella vulgaris*, wood and polypropylene through TGA, Bioresour. Technol. 243 (2017) 481–491.
[62] Q.V. Bach, W.H. Chen, Pyrolysis characteristics and kinetics of microalgae via thermogravimetric analysis (TGA): A state-of-the-art review, Bioresour. Technol. 246 (2017) 88–100.
[63] Soria-Verdugo, et al., Analyzing the pyrolysis kinetics of several microalgae species by various differential and integral isoconversional kinetic methods and the distributed activation energy model, Algal Res. 32 (2018) 11–29.
[64] X. Yang, et al., Pyrolysis kinetic and product analysis of different microalgal biomass by distributed activation energy model and pyrolysis–gas chromatography–mass spectrometry, Bioresour. Technol. 163 (2014) 335–342.
[65] D. López-González, et al., Pyrolysis of three different types of microalgae: kinetic and evolved gas analysis, Energy 73 (2014) 33–43.

[66] C. Liu, et al., Investigations on pyrolysis of microalgae Diplosphaera sp. MM1 by TG-FTIR and Py-GC/MS: Products and kinetics, Bioresour. Technol. 294 (2019) 122126.
[67] D. López-González, et al., Comparison of the steam gasification performance of three species of microalgae by thermogravimetric–mass spectrometric analysis, Fuel 134 (2014) 1–10.
[68] X. Wu, et al., Study on pyrolytic kinetics and behavior: The co-pyrolysis of microalgae and polypropylene, Bioresour. Technol. 192 (2015) 522–528.
[69] D.K.W. Gan, et al., Kinetics and thermodynamic analysis in one-pot pyrolysis of rice hull using renewable calcium oxide based catalysts, Bioresour. Technol. 265 (2018) 180–190.
[70] M.S. Ahmad, et al., Bioenergy potential of *Wolffia arrhiza* appraised through pyrolysis, kinetics, thermodynamics parameters and TG-FTIR-MS study of the evolved gases, Bioresour. Technol. 253 (2018) 297–303.
[71] J. Huang, et al., Combustion behaviors of spent mushroom substrate using TG-MS and TG-FTIR: Thermal conversion, kinetic, thermodynamic and emission analyses, Bioresour. Technol. 266 (2018) 389–397.
[72] G. Özsin, A.E. Pütün, TGA/MS/FT-IR study for kinetic evaluation and evolved gas analysis of a biomass/PVC co-pyrolysis process, Energy Convers. Manage. 182 (2019) 143–153.
[73] G.D. Mumbach, et al., Thermal investigation of plastic solid waste pyrolysis via the deconvolution technique using the asymmetric double sigmoidal function: Determination of the kinetic triplet, thermodynamic parameters, thermal lifetime and pyrolytic oil composition for clean energy recovery, Energy Convers. Manage. 200 (2019) 112031.
[74] A. Awasthi, et al., Production of phenolic compounds using waste coir pith: Estimation of kinetic and thermodynamic parameters, Bioresour. Technol. 274 (2019) 173–179.
[75] A. Fernandez, et al., Kinetic analysis and thermodynamics properties of air/steam gasification of agriculture waste, J. Environ. Chem. Eng. 8 (4) (2020) 103829.
[76] W. Ma, et al., The fate of chlorine during MSW incineration: Vaporization, transformation, deposition, corrosion and remedies, Prog. Energy Combust. Sci. 76 (2020) 100789.
[77] A. Gaeta-Bernardi, V. Parente, Organic municipal solid waste (MSW) as feedstock for biodiesel production: A financial feasibility analysis, Renew. Energy 86 (2016) 1422–1432.
[78] A. Johari, et al., Municipal solid waste management and potential revenue from recycling in Malaysia, Mod. Appl. Sci. 8 (4) (2014) 37–49.
[79] A.T. Sipra, N. Gao, H. Sarwar, Municipal solid waste (MSW) pyrolysis for bio-fuel production: A review of effects of MSW components and catalysts, Fuel Process. Technol. 175 (2018) 131–147.
[80] Plastic Europe, An Analysis of European Plastic Production, Demand and Waste Data, Association of Plastics Manufacturers, 2015, https://www.plasticseurope.org/application/files/5515/1689/9220/2014plastics_the_facts_Pub2015.pdf. (Accessed 1 April 2020).
[81] A. Oasmaa, et al., Pyrolysis of plastic waste: opportunities and challenges, J. Anal. Appl. Pyrolysis (2020) 104804.
[82] W. D'Ambrières, Plastics recycling worldwide: current overview and desirable changes Field Actions, Sci. Rep. 19 (2019) 12–21.
[83] A.A.P. Susastriawan, A.S. Purnomo, Experimental study the influence of zeolite size on low-temperature pyrolysis of low-density polyethylene plastic waste, Therm. Sci. Eng. Prog. 17 (2020) 100497.
[84] I. Ahmad, et al., Pyrolysis study of polypropylene and polyethylene into premium oil products, Int. J. Green Energy 12 (7) (2015) 663–671.
[85] J. Aguado, et al., Feedstock recycling of polyethylene in a two-step thermo-catalytic reaction system, J. Anal. Appl. Pyrolysis 79 (1) (2007) 415–423.
[86] Q. Hu, et al., Thermal behavior, kinetics and gas evolution characteristics for the co-pyrolysis of real-world plastic and tyre wastes, J. Clean. Prod. 260 (2020) 121102.
[87] B.L.F. Chin, et al., Comparative studies on catalytic and non-catalytic co-gasification of rubber seed shell and high-density polyethylene mixtures, J. Clean. Prod. 70 (2014) 303–314.
[88] R. Chen, et al., Insight into synergistic effects of biomass-polypropylene co-pyrolysis using representative biomass constituents, Bioresour. Technol. 307 (2020) 123243-123250.
[89] T. Kuppens, et al., Economic assessment of flash co-pyrolysis of short rotation coppice and biopolymer waste streams, J. Environ. Manag. 91 (12) (2020) 2736–2747.
[90] R. Chen, et al., Comparative study on synergistic effects in co-pyrolysis of tobacco stalk with polymer wastes: Thermal behavior, gas formation, and kinetics, Bioresour. Technol. 292 (2019) 121970-121979.
[91] X. Wang, et al., Synergistic effects of biomass and polyurethane co-pyrolysis on the yield, reactivity, and heating value of biochar at high temperatures, Fuel Process. Technol. 194 (2019) 106127-106137.
[92] F. Pinto, 98/02808 Co-pyrolysis of biomass with plastics: Pinto, F., et al., Dev. thermochem., Biomass Convers. 1 (1997) 229–241, Fuel and Energy Abstracts, 1998. 39(4):p. 260.
[93] E. Önal, et al., Bio-oil production via co-pyrolysis of almond shell as biomass and high density polyethylene, Energy Convers. Manage. 78 (2014) 704–710.
[94] N. Grioui, K. Halouani, F.A. Agblevor, Assessment of upgrading ability and limitations of slow co-pyrolysis: Case of olive mill wastewater sludge/waste tires slow co-pyrolysis, Waste Manage. 92 (2019) 75–88.
[95] S. Singh Siwal, et al., Energy production from steam gasification processes and parameters that contemplate in biomass gasifier – A review, Bioresour. Technol. 297 (2020) 122481.
[96] Z. Zhang, et al., Jet fuel range hydrocarbons production through competitive pathways of hydrocracking and isomerization over HPW-Ni/MCM-41 catalyst, Fuel 269 (2020) 117465.
[97] Y. Xue, X. Bai, Synergistic enhancement of product quality through fast co-pyrolysis of acid pretreated biomass and waste plastic, Energy Convers. Manage. 164 (2018) 629–638.
[98] J. Chattopadhyay, et al., Catalytic co-pyrolysis of paper biomass and plastic mixtures (HDPE (high density polyethylene), PP (polypropylene) and PET (polyethylene terephthalate)) and product analysis, Energy 103 (2016) 513–521.
[99] Q. Jin, X. Wang, et al., Synergistic effects during co-pyrolysis of biomass and plastic: gas, tar, soot, char products and thermogravimetric study, J. Energy Inst. 92 (1) (2019) 108–117.
[100] W. Chen, et al., Fast co-pyrolysis of waste newspaper with high-density polyethylene for high yields of alcohols and hydrocarbons, Waste Manage. 67 (2017) 155–162.
[101] Q.V. Nguyen, et al., Improvement of bio-crude oil properties via co-pyrolysis of pine sawdust and waste polystyrene foam, J. Environ. Manag. 237 (2019) 24–29.
[102] R.K. Mishra, et al., Pyrolysis kinetics and synergistic effect in co-pyrolysis of samanea saman seeds and polyethylene terephthalate using thermogravimetric analyser, Bioresour. Technol. 289 (2019) 121608.
[103] M.J. Starink, The determination of activation energy from linear heating rate experiments: a comparison of the accuracy of isoconversion methods, Thermochim. Acta 404 (1) (2003) 163–176.
[104] P. Supaphol, J.E. Spruiell, Kinetics of non-isothermal crystallization syndiotactic polypropylene: Avrami, Ozawa, and Kissinger approaches, in: G.M. Benedikt (Ed.), Metallocene Technology in Commercial Applications, William Andrew Publishing, Norwich, NY, 1999, pp. 263–273.
[105] H.E. Kissinger, Reaction kinetics in differential thermal analysis, Anal. Chem. 29 (11) (1957) 1702–1706.
[106] J.H. Flynn, L.A. Wall, A quick, direct method for the determination of activation energy from thermogravimetric data, J. Polymer Sci. B Polymer Lett. 5 (5) (1966) 323–328.
[107] O. Takeo, A new method of analyzing thermogravimetric data, Bull. Chem. Soc. Jpn. 38 (11) (1965) 1881–1886.
[108] P. Chaiwang, B. Chalermsinsuwan, P. Piumsomboon, Thermogravimetric analysis and chemical kinetics for regeneration of sodium and potassium carbonate solid sorbents, Chem. Eng. Commun. 203 (5) (2016) 581–588.
[109] S. Vyazovkin, et al., ICTAC Kinetics Committee recommendations for performing kinetic computations on thermal analysis data, Thermochim. Acta 520 (1) (2011) 1–19.
[110] I. Ali, A. Bahadar, Thermogravimetric characteristics and non-isothermal kinetics of macro-algae with an emphasis on the possible partial gasification at higher temperatures, Front. Energy Res. 7 (7) (2019).
[111] M. Aghbashlo, et al., Prognostication of lignocellulosic biomass pyrolysis behavior using ANFIS model tuned by PSO algorithm, Fuel 253 (2019) 189–198.
[112] X. Zhang, W. de Jong, F. Preto, Estimating kinetic parameters in TGA using B-spline smoothing and the friedman method, Biomass Bioenergy 33 (10) (2009) 1435–1441.
[113] J.A. Huidobro, et al., Reducing the effects of noise in the calculation of activation energy by the Friedman method, Chemometr. Intell. Lab. Syst. 151 (2016) 146–152.
[114] M.J. Starink, Analysis of hydrogen desorption from linear heating experiments: Accuracy of activation energy determinations, Int. J. Hydrogen Energy 43 (13) (2018) 6632–6641.
[115] J.A. Vara, P.N. Dave, S. Chaturvedi, The catalytic activity of transition metal oxide nanoparticles on thermal decomposition of ammonium perchlorate, Def. Technol. 15 (4) (2019) 629–635.
[116] J. Liu, et al., Preparation of biochar from food waste digestate: Pyrolysis behavior and product properties, Bioresour. Technol. 302 (2020) 122841.
[117] X. Fang, L. Jia, L. Yin, A weighted average global process model based on two-stage kinetic scheme for biomass combustion, Biomass Bioenergy 48 (2013) 43–50.
[118] S. Hameed, et al., A review on biomass pyrolysis models: Kinetic, network and mechanistic models, Biomass Bioenergy 123 (2019) 104–122.
[119] Y. Lin, et al., General distributed activation energy model (G-DAEM) on co-pyrolysis kinetics of bagasse and sewage sludge, Bioresour. Technol. 273 (2019) 545–555.
[120] D.K. Shen, et al., Thermal degradation mechanisms of wood under inert and oxidative environments using DAEM methods, Bioresour. Technol. 102 (2) 2047–2052.
[121] M. Güneş, S. Güneş, A direct search method for determination of DAEM kinetic parameters from nonisothermal TGA data (note), Appl. Math. Comput. 130 (2) (2002) 619–628.

[122] S. Vyazovkin, et al., ICTAC Kinetics Committee recommendations for collecting experimental thermal analysis data for kinetic computations, Thermochim. Acta 590 (2014) 1–23.
[123] S.V. Vyazovkin, A.I. Lesnikovich, The use of non-linear statistic methods for determination of kinetic parameters and kinetic functions choise according to thermogravimetric data, Thermochim. Acta 92 (1985) 161–164.
[124] C.F. Dickinson, G.R. Heal, A review of the ICTAC kinetics project , 2000: Part 2. Non-isothermal result, Thermochim. Acta 494 (1) (2009) 15–25.
[125] J. Cai, et al., A distributed activation energy model for the pyrolysis of lignocellulosic biomass, Green Chem. 15 (5) (2013) 1331–1340.
[126] J. Cai, L.Q. Ji, Pattern search method for determination of DAEM kinetic parameters from non-isothermal TGA data of biomass, J. Math. Chem. 42 (3) (2007) 547–553.
[127] National Math and Science Initiative, 2014, Enthalpy, Entropy and Free Energy, 2014.
[128] K.O. Stanley, J. Clune, J. J. Lehman, R. Miikkulainen, Designing neural networks through neuroevolution, Nat. Mach. Intell. 1 (1) (2019) 24–35.
[129] D.P. Kingma, J. Ba, Adam: A method for stochastic optimization, 2014, arXiv preprint arXiv:1412.6980.
[130] Y. Shi, R. Eberhart, A modified particle swarm optimizer, in: 1998 IEEE International Conference on Evolutionary Computation Proceedings. IEEE World Congress on Computational Intelligence (Cat. No. 98TH8360), IEEE, 1998, pp. 69–73.
[131] Z. Lu, I. Whalen, V. Boddeti, Y. Dhebar, K. Deb, E. Goodman, W. Banzhaf, Nsga-net: neural architecture search using multi-objective genetic algorithm, in: Proceedings of the Genetic and Evolutionary Computation Conference, 2019, pp. 419–427.
[132] S. Kirkpatrick, C.D. Gelatt, M.P. Vecchi, Optimization by simulated annealing, Science 220 (4598) (1983) 671–680.
[133] B.W. Zhao, X. Wang, X.Y. Yang, Co-pyrolysis characteristics of microalgae Isochrysis and Chlorella : kinetics, biocrude yield and interaction, Bioresour. Technol. 198 (2015) 332–339.
[134] Z.H. Chen, et al., Characteristics and kinetic study on pyrolysis of five lignocellulosic biomass via thermogravimetric analysis, Bioresour. Technol. 192 (2015) 441–450.
[135] C. Gai, et al., Thermogravimetric and kinetic analysis of thermal decomposition characteristics of low-lipid microalgae, Bioresour. Technol. 150 (2013) 139–148.
[136] R.K. Mishra, K. Mohanty, Pyrolysis kinetics and thermal behavior of waste sawdust biomass using thermogravimetric analysis, Bioresour. Technol. 251 (2018) 63–74.
[137] P.A. Bartocci, et al., Pyrolysis of pellets made with biomass and glycerol: kinetic analysis and evolved gas analysis, Biomass Bioenergy 97 (2017) 11–19.
[138] Y.J. Rueda-Ordóñez, K. Tannous, Isoconversional kinetic study of the thermal decomposition of sugarcane straw for thermal conversion processes, Bioresour. Technol. 196 (2015) 1–9.
[139] A. Dewangan, D. Pradhan, R.K. Singh, Co-pyrolysis of sugarcane bagasse and low-density polyethylene: influence of plastic on pyrolysis product yield, Fuel 185 (2016) 508–516.
[140] B. Han, et al., Co-pyrolysis behaviors and kinetics of plastics-biomass blends through thermogravimetric analysis, J. Therm. Anal. Calorim. 115 (2014) 227–235.
[141] A.S. Burange, et al., Heterogeneously catalyzed strategies for the deconstruction of high density polyethylene: plastic waste valorisation to fuels, Green Chem. 17 (1) (2015) 146–156.
[142] X.P. Kai, et al., TG-FTIR-MS study of synergistic effects during co-pyrolysis of corn stalk and high-density polyethylene (HDPE), Energy Convers. Manage. 181 (2) (2019) 202–213.
[143] X.S. Zhang, H.W. Lei, S.L. Chen, J. Wu, Catalytic co-pyrolysis of lignocellulosic biomass with polymers: a critical review, Green Chem. 18 (15) (2016) 4145–4169.
[144] F. Fan, et al., In-situ degradation of polybrominated diphenyl ethers from thermal desorption off-gas over structured Fe-based/γ-Al_2O_3/Al plate-type catalyst, J. Hazard. Mater. 384 (2020) 121251.
[145] Y. Shi, et al., Synergistic effect of Pt/Ce and USY zeolite in Pt-based catalysts with high activity for VOCs degradation, Appl. Catal. B 286 (2021) 119936.
[146] Y. Fan, et al., Low temperature catalytic degradation of chlorinated aromatic hydrocarbons over bimetallic Ce-Zr/UiO-66 catalysts, Chem. Eng. J. 414 (2021) 128782.
[147] S. Zafar, Biomass pyrolysis, solar & wind biomass energy, 2009, https://www.altenergymag.com/article/2009/02/biomass-pyrolysis/502/. (Accessed 15 August 2020).
[148] K. Miura, T. Maki, A simple method for estimating f(E) and k0(E) in the distributed activation energy model, Energy & Fuels (11) (1998) 864–869.
[149] F.S.M. Sinfrônio, et al., Kinetic of thermal degradation of low-density and high-density polyethylene by non-isothermal thermogravimetry, J. Therm. Anal. Calorim. 79 (2) (2005) 393–399.
[150] I. Kayacan, Ö.M. Doğan, Pyrolysis of low and high density polyethylene. part I: non-isothermal pyrolysis kinetics, Energy Sources A Recovery Utilization Environ. Eff. 30 (2008) 385–391.
[151] M.S. Ahmad, M.A. Mehmood, et al., Pyrolysis, kinetics analysis, thermodynamics parameters and reaction mechanism of Typha latifolia to evaluate its bioenergy potential, Bioresour. Technol. 245 (2017) 491–501.
[152] D. Yu, H. Hui, S. Li, Two-step catalytic co-pyrolysis of walnut shell and LDPE for aromatic-rich oil, Energy Convers. Manage. 198 (2019) 111816.